The copyright of this thesis vests in the author. No quotation from it or information derived from it is to be published without full acknowledgement of the source. The thesis is to be used for private study or non-commercial research purposes only.

Published by the University of Cape Town (UCT) in terms of the non-exclusive license granted to UCT by the author.

University of Cape Town

Department of Human Biology

Biomedical Engineering

fMRI Guided DTI at the Grey-White Matter Interface

With Application to a Connectivity Analysis of the Default Mode Network in Urbach-Wiethe Disease

MSc Thesis

Author:

Roland Baasch

BSCROL001

Supervisors:

Dr. Bruce Spottiswoode

Dr. Barak Morgan

In fulfillment of the degree

Master of Science in Medicine in Biomedical Engineering

MSc(Med)(BME)

May 27, 2011

University of Cape Town

Contents

University of Cape Town

List of Figures

University of Cape Town

University of Cape Town

List of Tables

University of Cape Town

List of Abbreviations

BLA Basolateral Amygdala

BOLD Blood Oxygen Level Dependant

CB Cingulum Bundle

CB Cingulum Bundle

CMA Centromedial Amygdala

CST Corticospinal Tract

DMN Default Mode Network

DSI Diffusion Spectrum Imaging

EPI Echo-Planar Images

FA Fractional Anisotropy

FACT Fibre Assignment by Continuous Tracking

fcMRI functional connectivity MRI

FDR False Discovery Rate

FM Fast Marching

University of Cape Town

fMRI Functional Magnetic resonance Imaging

FWE Family Wise Error

GLM General Linear Model

GM Grey Matter

HARDI High Angular Resolution Diffusion Imaging

HRF haemodynamic response function

ICA Independent Component Analysis

MD Mean Diffusivity

MRI Magnetic resonance Imaging

PCC Posterior Cingulate Cortex

PDD Principal Diffusion Direction

RAFF Radiality Flood-Fill

ROI Region of Interest

SFA Superficial Amygdala

SNR Signal to Noise Ratio

TBSS Tract Based Spatial Statistics

UWD Urbach-Wiethe Disease

WM White Matter

University of Cape Town

Declaration

I hereby declare that the work contained in this thesis is my own original work, except for material which has been referenced. This work has not previously in its entirety or in part been submitted at any university for a degree.

Signature: .. Signed by candidate .....

Date: 31/05/2011 .....

Abstract

The cerebral cortex is composed of a thin layer of Grey Matter (GM), functionally subdivided into discrete regions which are connected in a large scale network via White Matter (WM) tracts. With fMRI (Functional Magnetic Resonance Imaging) it is possible to identify cortical regions involved in specific tasks, and with DTI (Diffusion Tensor Imaging) the structural connections between these areas can be mapped. The aim of this thesis is to to identify and track only those WM tracts entering and leaving a GM Region Of Interest (ROI) defined by fMRI. Since fMRI is confined to GM and DTI outside the WM can be problematic, the major challenge lies in selecting and following the correct DTI signals at the GM/WM interface. A flood-fill algorithm based on a metric which exploits the radial structure of axons at the GM/WM boundary is used to grow fMRI ROIs into the WM to allow for effective DTI tractography. Quantitative validation using Cohen's kappa shows a high degree of agreement between the new automated technique and existing techniques which depend upon a manually (and therefore subjectively) defined ROI at the GM/WM interface. The flood-fill approach was then used to investigate Default Mode Network (DMN) connectivity in Urbach-Wiethe Disease (UWD), an extremely rare genetic condition characterised by selective bilateral amygdala calcification. Intact social, emotional and intellectual function suggests that WM connections not directly associated with the amygdala have remained intact. This hypothesis was investigated by comparing the Cingulum Bundle of UWD subjects to matched controls.

University of Cape Town

Acknowledgments

Firstly, I would like to thank my supervisors, Bruce and Barak, for their support and encouragement in developing this thesis. Through your experience, I was exposed to many different aspects of neuroimaging.

Thanks to the staff and students at the Biomedical Engineering Department who provided the support and the background I needed to enter a new field. I also would like to thank my family and friends and especially my girlfriend Gina for motivating me and giving me the confidence I needed to take on a Masters degree.

Lastly, I would like to acknowledge the National Research Foundation of South Africa for funding assistance.

Chapter 1

Introduction

"Neurons that fire together, wire together."- Hebb's Law (paraphrased)

1.1 Problem Description

Diffusion tensor imaging (DTI) and functional magnetic resonance imaging (fMRI) are two MRI techniques capable of measuring very different physiological properties. DTI can be used to indirectly infer the anatomical links between brain regions by tracking the white matter which connects them. fMRI measures fluctuations in regional blood flow to infer regional brain activity. The use of DTI in clinical and research settings is gaining popularity as the data acquisition and processing techniques improve. However, current methods of DTI require expert knowledge and are also subject to some degree of subjectivity. The reconstructed tract pathways depend heavily on the location of the fibre tracking seeds, which define the initiation points for fibre tracking (tractography). User seed placement requires expert knowledge of white matter anatomy. This work attempts to overcome these problems by coregistering fMRI with DTI data, and using regions identified by fMRI to initialise the extraction of the associated white matter connections. Several attempts have been made to do this but these still require manual intervention which again would introduce variable results. Since the fMRI activation is confined to the grey matter and DTI largely to the

white matter, these studies manually manipulated the fMRI edges to ensure that they extended into the white matter to allow for tractography. The utility of combining fMRI with DTI would be greatly enhanced by a reliable, automated method of crossing the grey/white matter boundary.

1.2 Research Aims

The primary aim of this work is to develop an automated method to combine the information from DTI and fMRI in a way that allows reliable extraction of white matter tracts. The use of DTI in research and clinical neuroscience is a relatively qualitative and subjective task requiring anatomical knowledge of the white matter pathways of the brain. By applying knowledge of how the fibre tracts interact with the cortical anatomy, based on cytoarchitectural evidence, fMRI seeds can be made to "grow" into regions that produce more reliable white matter fibre tracking results.

The second aim of this thesis is to investigate white matter differences in the brains of Urbach-Wiethe disease subjects compared to healthy controls. This non-neurodegenerative disease is of special interest since it is the only human model of a highly stable, selective, focal bilateral lesion anywhere in the brain. The amygdala is an extensively interconnected brain region and the effects of this lesion on the global brain connections are not fully understood.

1.3 Thesis Outline

The primary and secondary aims of the thesis are separated into two distinct parts. Chapter 2 provides some background to the basics of DTI and fMRI data acquisition, processing and analysis. The methods and limitations in the current practice of analysing brain connectivity from DTI data are presented in the context of combining fMRI with DTI. The structural and micro-structural architecture of the grey and white matter of the brain which lead to the proposed method used in the analysis are also described. Finally the methods employed

for the validation framework in resting state fMRI are described.

Chapter 3 applies the methods introduced in Chapter 2 in a case study using data from an ongoing investigation into white matter connectivity in Urbach-Wiethe disease. Chapter 4 then presents a discussion of the methods described and results generated and a conclusion with recommendations for future work.

1.4 Scope and Limitations

This thesis assumes that the reader understands the basic principles of MRI physics and image processing. For the clinical case study, it assumes that the reader does not have knowledge of neuropsychology, and presents a basic background in the anatomy and function of the Default Mode Network, and on Urbach-Wiethe disease.

This is an investigation into how fMRI data can be used in a DTI work-flow to extract tracts underlying the fMRI activity. The success of extracting reliable fMRI derived tracts from DTI, judged by measuring the agreement of the resulting tracts with those achieved using standard protocols, depends on several factors:

i. the reliability of fMRI.

ii. the quality of the coregistration.

iii. the trajectory of the tract of interest relative to other anatomy.

iv. the effectiveness of the seeding strategy.

The effectiveness of the proposed seeding strategy is assessed by assuming that items i. to iii. are held constant. The scope of the work is thus defined by the following three constraints: i. using individual rather than group fMRI analysis, ii. limiting coregistration to an intra-subject rigid body transformation, and iii. only looking at specific tracts.

University of Cape Town

The fundamental limitation in this thesis is the inability to track fibre pathways reliably into the grey matter of the brain. There is a breakdown in the information contained in the DTI data as the tract approaches the tissue interface due to partial volume effects and low spatial resolution. Deterministic fibre tracking was employed in this thesis rather than probabilistic methods. Deterministic tracking might be less suitable than some of the available fibre tracking methods to track fibres in these boundary regions, however, it is the most commonly used in clinical and academic settings. It is the goal of this thesis to overcome these limitations, and to track reliably using the deterministic tractography framework at the tissue interface from regions defined by fMRI.

There is no true gold-standard upon which one can validate DTI tractography so validation employed here is based on current practice, which may still introduce some subjectivity in the evaluation of the tracts.

The relatively low resolution and the limitations of the DTI model have raised questions as to its ability to reveal thin and short fibres, or the fibres in complex regions (e.g crossing or touching tracts). Because of this, the investigation was limited to certain major tracts (the Cingulum Bundle and Corticospinal tract).

University of Cape Town

Chapter 2

Developing an Approach for Combining fMRI and DTI

2.1 Introduction

In this chapter, the motivation for combining fMRI with the DTI processing pipeline is presented. A method based on extending the initial fMRI Regions Of Interest (ROI's) into the white matter using a flood-fill based on local diffusion properties at the GM/WM tissue boundary, is described. fMRI was first conducted using a motor task to define the motor cortex and hence the Corticospinal Tract (CST). Resting state fMRI data were also acquired, and, a major interconnecting tract, the Cingulum Bundle was extracted from Default Mode Network activation in each individual subject. The fMRI-based approach is validated by comparing the resulting tracts to the tracts derived from a standard method, and using Cohen's kappa to quantify the accuracy. The data processing pipeline is summarised in Figure 2.1.

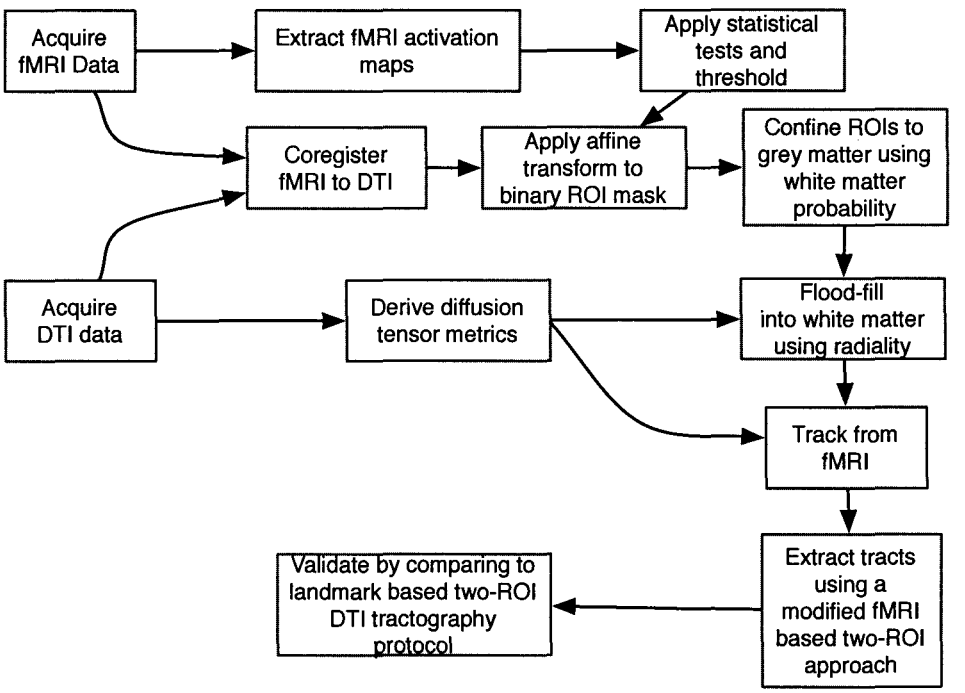

Figure 2.1: Data processing pipeline summarising the steps involved in Chapter 2.

2.2 Background

2.2.1 Functional MRI

The basic fMRI experiment has the subject in the scanner perform a series of cognitive tasks. The task paradigm is designed to compare epochs or events of interest with control or rest epochs or events. A brain volume image is typically acquired every 2-3 s throughout the duration of the task. Hundreds of brain volumes may be accumulated during the execution of a complete fMRI scan, lasting between 2 and 10 minutes. Typical resolutions of 3×3×3 mm^3 are achieved in standard fMRI sequences.

When neurons are activated, there is an increased need for oxygen and this results in an increase in blood perfusion. Functional MRI (fMRI) is sensitive to this perfusion change via the Blood Oxygen Level Dependant (BOLD) principle which arises from the magnetic properties of haemoglobin and deoxyhaemoglobin. Oxygenated haemoglobin has very little

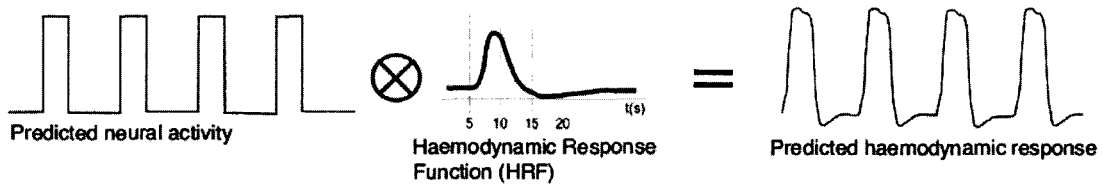

Figure 2.2: The haemodynamic response to a neural event can be used to model the predicted response to a block design fMRI paradigm.

effect on the magnetic field in an MRI scanner. As oxygen is lost to the tissue as blood passes through the tissue via the capillaries, oxyhaemoglobin becomes deoxyhaemoglobin, which disrupts the MRI signal in proportion to the amount of oxygen lost. There is a link between neural activity and the measured T2* signal and this is called the BOLD contrast mechanism. As brain activity increases, blood flow and glucose consumption increase much more that oxygen consumption and as a result, the amount of deoxyhaemoglobin decreases in areas of increased metabolic activity, and the BOLD signal is increased proportionally. The opposite occurs when activity decreases. The BOLD response occurs mostly in the grey matter, since there is far greater energy metabolism and vascularisation than in white matter (Logothetis and Wandell, 2004). The BOLD signal is related to neuronal stimulus by the haemodynamic response function (HRF) which is shown in Figure 2.2 relative to a hypothetical impulse stimulus.

The analysis of the fMRI data consists of two stages: (1.) preprocessing and (2.) statistical analysis. Preprocessing involves preparation of the data by smoothing, applying slice-timing correction and motion correction. Statistical measures can then be applied to estimate the degree of relative increase or decrease in neuronal activity. In "block" fMRI designs the tasks performed in the scanner ensure cognitive engagement by sequentially presenting stimuli in predefined blocks. A canonical HRF is convolved with the task design to create the General Linear Model (GLM) to predict the neural response. This predicted BOLD response within each voxel is used as a regressor and fitted to the measured BOLD signal response (Figure 2.2). Any signal changes are statistically tested for significance. The length of the blocks of stimulation should allow for the HRF to reach maximal values, while the rest intervals should be long enough for the HRF to return completely to baseline during non-stimulation.

Resting State Functional Connectivity

Resting state fMRI is a relatively new area of research which does not require a predicted response. When performing fMRI in the absence of a task, specific brain regions show synchronised activity, which suggests that they are functionally connected (Uddin *et al.*, 2010). Even at rest, spontaneous BOLD activity is evident, showing increasing power at lower frequencies. The power spectral density curve exhibits a 1/frequency behaviour, meaning most of the power is concentrated in the low frequency range of the total power spectrum. Large clusters of neurons form functional networks which are held together by the neurons' synchronised firing. These slow fluctuations (<0.1 Hz) show patterns of coherence across known networks in the brain (Fox and Raichle, 2007). These regions are continuously sharing information with each other over a complex neural network (Friston *et al.*, 1993a). The activation patterns in the brain tend to be spatially smooth and clustered (Li *et al.*, 2007). Investigative techniques such as Independent Component Analysis (ICA) are able to resolve the multiple components of signal and noise from a single source. When ICA is be applied to fMRI data, it identifies functionally connected regions based on their temporal (through the BOLD time-course) and spatial (regions that are near to each other tend to have more similar values) correlations. This analysis is known as fcMRI (functional connectivity MRI) (Cohen *et al.*, 2008). ICA has been demonstrated to be effective in studying brain function since it is data-driven and makes no assumptions of the underlying anatomy when capable of separating the neuronal signal components from the underlying noise of the fMRI signal. It is therefore suitable for application when regions involved in a specific task are not known or when data are acquired in the resting state. fcMRI allows several distinct resting state networks to be detected at once, where the components extracted represent independent networks (Greicius, 2008). The resting state literature has identified around eight reliably extracted resting state networks. These include the motor network, visual network, Default Mode Network (DMN) and other attentional networks.

Consistent activation patterns have been demonstrated on a variety of different scanners and using seed based, clustering analysis methods and ICA. In addition, a Corpus Callosum section study by Johnston *et al.* (2008) used seed based functional connectivity analysis to show a striking loss of inter-hemispherical connectivity, while maintaining intra-hemispheric correlations postoperatively. This study also showed that the non-neuronal effects account for

University of Cape Town

less than 11% of the total BOLD signal coherence. Inter-hemispheric functional connectivity is maintained by the interconnecting neuronal pathways of the Corpus Callosum.

The Default Mode Network

The Default Mode Network (DMN) is unique amongst the resting state networks in that it deactivates in response to cognitive tasks (Buckner *et al.*, 2008). Figure 2.3 shows the typical activation pattern of the DMN. The activated regions include the medial Prefrontal Cortex (mPFC) and Posterior Cingulate Cortex (PCC), which are the large mid-line structures showing the highest activity. Analysis of resting state fMRI data has been used to show differences in DMN activity in clinical populations indicating differences in intrinsic brain function (Broyd *et al.*, 2009).

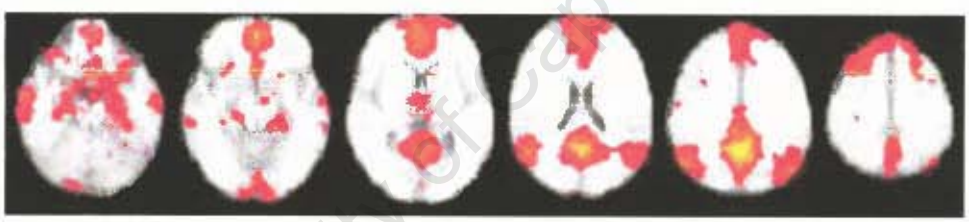

Figure 2.3: The typical DMN activation pattern is evident in this axial view of fMRI data.

University of Cape Town

2.2.2 Diffusion Tensor Imaging

DTI is a non-invasive technique which is able to quantify the diffusion of water by applying bipolar magnetic field gradients to the water molecules. Random movement of water molecules occurs by Brownian motion caused by internal thermal energy. In certain tissues the movement of water molecules is limited by the tissue structure, reducing the ability to diffuse freely. When the water molecules move by random motion due to thermal energy, a signal reduction is seen which provides a measure of diffusion in the magnetic gradient direction. By measuring the preferred direction of diffusion it is possible to reconstruct the underlying structure of the tissue. Before the advent of DTI, earlier techniques of finding axonal connection patterns involved postmortem histological study, or required the injection of potentially harmful tracers before imaging. Although this cannot be applied to humans *in*

vivo, postmortem and tracer studies remain the gold standard for validation (Kim and Kim, 2005). The direction of the gradient fields are changed during the scan to encode diffusion in multiple directions in each voxel (volumetric pixel). The Diffusion Weighted (DW) signal is obtained using the Stejskal-Tanner equation:

$$S = S_0 \times e^{-bD} \tag{2.1}$$

$$b[s/mm^2], D[mm^2/s],$$

where S_0 is the signal intensity without diffusion weighting (no gradient applied) and S is the signal with the gradient application. Here $b = \gamma^2 G^2 \delta^2 (\Delta - \delta/3)$, where γ is the gyromagnetic constant, G is the bipolar gradient amplitude, δ is the duration of the gradients and Δ is the amount of time between the bipolar gradient lobes. The diffusion, D, varies from voxel to voxel, and defines the apparent diffusion. This is described by a diffusion tensor.

By rearranging Equation 2.1 by solving for D and applying at least 6 non-collinear gradients, we obtain a 3×3 matrix which characterises the three dimensional movement of water (defined in the Cartesian coordinates x, y and z). This represents the diffusion tensor:

$$\underline{\underline{D}} = \begin{bmatrix} D_{xx} & D_{yx} & D_{zx} \\ D_{xy} & D_{yy} & D_{zy} \\ D_{xz} & D_{yz} & D_{zz} \end{bmatrix} \tag{2.2}$$

In each voxel the tensor can be represented as an ellipsoid with the largest of the tensor eigenvectors representing the Principal Diffusion Direction (PDD), as shown in Figure 2.4. Structures such as cell membranes and myelin sheaths constrain the movement of water in highly ordered tissues such as the white matter of the brain. The geometry of the ellipsoid shows the direction of the ordered fibres. The main axis of the ellipsoid is the largest eigenvector of the tensor, which corresponds to the axonal direction. Scalar measures derived from the tensor can provide quantitative information about the underlying tissue structure.

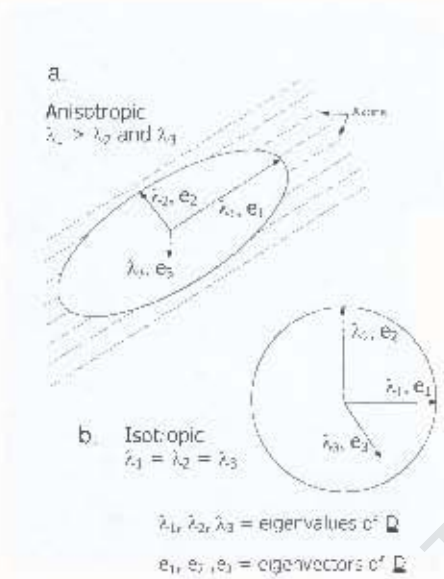

Figure 2.4: Diffusion tensor representations for (a.) anisotropic and (b.) isotropic scenarios. In areas with anisotropic diffusion, the principal eigenvector λ_1 is taken as the Principal Diffusion Direction (PDD). $\underline{\underline{D}}$ is the diffusion tensor.

Fractional Anisotropy (FA) is defined as the normalised standard deviation of the eigenvalues and represents tissue anisotropy. Recent findings indicate that FA is a reliable microstructural marker of tract integrity which underlies neuronal network connectivity (Teipel *et al.*, 2010). Figure 2.5 shows an example of an FA map. Mean Diffusivity (MD) is a measure of the average diffusivity of the water in a voxel and is invariant to orientation. MD and FA are defined as:

$$MD = \frac{\lambda_1 + \lambda_2 - \lambda_3}{3} \tag{2.3}$$

$$FA = \sqrt{\frac{3}{2}} \frac{\sqrt{(\lambda_1 - MD)^2 - (\lambda_2 - MD)^2 + (\lambda_3 - MD)^2}}{\sqrt{(\lambda_1 + \lambda_2 + \lambda_3)}} \tag{2.4}$$

where $\lambda_1, \lambda_2 \text{and} \lambda_3$ are the eigenvectors of the diffusion tensor $\underline{\underline{D}}$. High FA is found in highly ordered regions such as white matter, which is usually defined as FA ≥ 0.2 (Mori and van Zijl, 2002). Low FA values occur in the grey matter due to the branching of the white matter

University of Cape Town

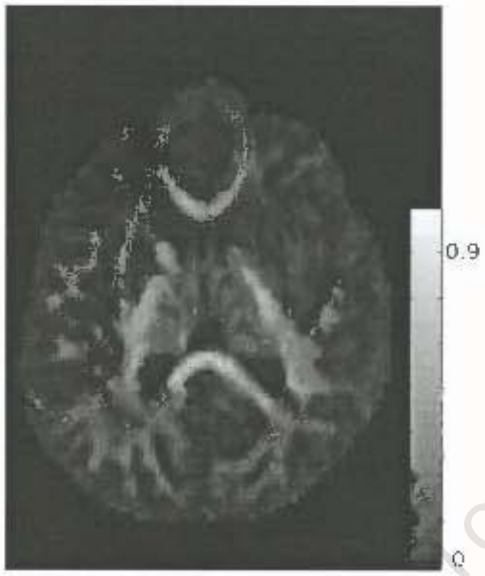

Figure 2.5: An axial view of an FA map, which represents the level of anisotropy of the diffusion signal.

as it enters/leaves the neurons of the grey matter layer. As a result, the diffusion of water becomes less limited by cellular constraints and the microscopic tissue obstructions become less collinear. FA in the grey matter is usually in the range 0.1 - 0.2. In the centre of tightly packed white matter bundles, the FA approaches 1 and appears bright on an FA map.

A lowered FA in the white matter may be due to tissue breakdown where the cellular integrity is reduced, for example, by myelin degeneration, stroke or other pathology. The FA metric can be used to quantitatively describe the integrity of specific white matter regions (Rykhlevskaia *et al.*, 2008). FA increases with the degree of myelination, axonal thickness, amount of parallel organisation of axons, or a combination of these factors. The ability of the axon to transport action potentials is dependent on these factors and so FA also provides an indirect measure of white matter efficiency (ability to transmit information). Each white matter voxel consists of thousands of axons (neuronal projections) and of various kinds of glial cells (supporting cells) and myelin sheaths. The myelin envelops the axons and ensures fast and efficient transmission of electrical signals through them. They are also the major cellular component limiting the diffusion of water (Assaf and Pasternak, 2008).

University of Cape Town

Figure 2.6: A colour coded FA map showing the PDD vectors in the vicinity of the genu of the Corpus Callosum. Red = right-left, blue = inferior-superior and green = anterior-posterior. The PDD vector has also been scaled by FA.

Figure 2.6 shows a subsection of a colour-coded FA map with the principal eigenvectors overlaid. The directional information is encoded in red (right-left), blue (inferior-superior) and green (anterior-posterior) directions. The principal axis of the tensor fitted to each voxel describes the orientation of the white matter.

Tractography

Three dimensional reconstructions of white matter tracts can be generated by following the principal direction of water diffusion at each image voxel in the brain (Basser *et al.*, 2000). The process of reconstructing fibre paths from the tensor field is known as tractography. Tracking is initiated from predefined seed points and the pathways are interpolated to form

University of Cape Town

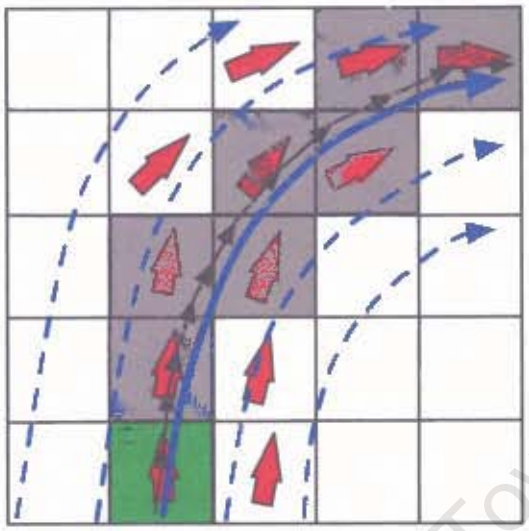

Figure 2.7: A two dimensional view of the FACT fibre tracking by line propagation is shown here. The principle eigenvector is represented as a red arrow in each pixel. A fibre path (blue) is generated by interpolating between the principal eigenvectors pixel by pixel. The seed point is indicated by the green pixel from which the black arrows show the continuous intercepts which assign the fibre path (adapted from (Mori *et al.*, 1999)).

a tract at sub-pixel resolution. It is important to remember that the fibre tracts resulting from tractography are only representations of the anatomy based on water diffusion. A variety of techniques exist for tracing the paths of axonal tracts using DTI data, but the most widely used is a deterministic line propagation approach to track the fibre by connecting each voxel to the adjacent one. However, this limits the path of the tract to only eight of its nearest neighbours and results in non-smooth, possibly erroneous trajectories. The Fibre Assignment by Continuous Tracking (FACT) algorithm improves on this limitation, using distance-weighted linear interpolation to propagate a streamline from an initial seed point in the direction of the principle eigenvector for small spatial increments (Mori *et al.*, 1999). The FACT process is depicted in Figure 2.7.

DTI provides a macroscopic view of the microstructure of the white matter axons, therefore with FACT it is often difficult to discern fibres crossing, merging, diverging or kissing (tracts merging and then diverging), within a particular voxel (Mori and van Zijl, 2002). The innovative use of High Angular Resolution Diffusion Imaging (HARDI) techniques which incorporates Diffusion Spectrum Imaging (DSI) and "Q-ball" imaging, seeks to resolve these

University of Cape Town

inherent resolution problems in DTI (Hagmann *et al.*, 2006). These techniques work by applying many diffusion gradients (sometimes > 200) and then quantifying the diffusion in each voxel by a probability density function. The gradients are applied uniformly over a sphere of radius q, the angular resolution is therefore only limited to the resolution in q-space. The axis of strongest diffusion is still depicted as in the ellipsoid tensor model, but now allows for the possibility of multiple directions within each voxel.

Probabilistic tractography algorithms based on the tensor model can also be applied to estimate tensor parameters based on global connectivity. In other words, they allow a measure of maximum probability of connection through the tensor field between two points, thus providing a measure of confidence in this pathway (Behrens *et al.*, 2003).

One such approach, known as Fast Marching (FM) is based on level set methods (Parker *et al.*, 2002). The FM method can be thought of as the motion of a front evolving from a source, which is dependent on a function based on the diffusion tensor. This allows for a probabilistic measurement of the likelihood of connection and also provides the ability to show a multitude of potential pathways, especially in regions where uncertainty is high (such as in the grey matter).

These advanced techniques require complex algorithms and extensive data processing. While DTI determines the tensor model by simple matrix operations, Q-ball and DSI require complex filtering and projection with multiple parameter settings. Because of the increased number of gradients needed, much longer scan times are required (Hagmann *et al.*, 2006). FACT is still by far the most commonly used tractography algorithm. It has been shown in some comparative fibre tracking studies, that the simple tracking methods produce similar results to the more complicated algorithms, especially in well defined networks with strong white matter connections (Fransson and Marrelec, 2008).

A brute force approach is commonly taken, where every voxel in the brain is used as a seed point. However, this is computationally expensive and results in a confusing amalgamation of large numbers of fibres. The user then has the task of trimming the fibres with logical

University of Cape Town

Boolean operations.

Fibre tracts initiated from discrete regions are highly dependent on seed or ROI placement. Studies comparing inter- and intra-rater variability of user-defined ROI placement show fairly good reproducibility in the resulting tracts (Wakana *et al.*, 2007), however this still depends heavily on user knowledge and assumes that the tract trajectory is known. In addition, tractography based on small ROIs including only a few voxels might be very sensitive to partial volume effects.

Isolating Specific Tracts Using Boolean Operators

A multiple ROI method, described by Mori and van Zijl (2002), uses Boolean operations to select specific tracts based on anatomical landmarks (landmark based two-ROI method . The AND (the tract must pass through all ROIs) and NOT (remove fibres passing through a ROI) functions are the most commonly applied operations. The basic idea is described in Figure 2.8. Tract identification using this method was formalised in Wakana *et al.* (2007) by providing anatomical landmarks on the vector colour maps for 11 of the major fibre systems of the brain. Consistent inter and intra-rater reproducibility was found for the two-ROI protocol. The landmark based two-ROI protocol for extracting the Cingulum Bundle (CB) is shown in Figure 2.9.

University of Cape Town

With prior knowledge of the tract of interest, the specificity of the tract is greatly increased by applying the second ROI, through which the tract trajectory is known to pass, and using a logical AND operator. Seeding also effects the resulting tractography, but any specificity gained by seeding from fMRI is masked by the extremely specific condition imposed by the AND operator. In addition, when conducting exploratory work, the second ROI isn't known *a priori*.

In this thesis, the isolation of a tract of interest using two manually defined ROIs (ROI 1 to provide seed points and a manually defined ROI 2, for the Boolean AND operation) is referred to as the "landmark based two-ROI method." This is in contrast with a simple

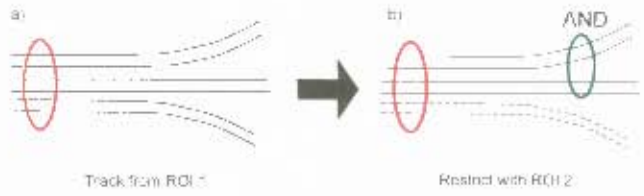

Figure 2.8: A schematic diagram illustrating a multiple ROI method using Boolean operations. Tracking is initiated from ROI 1. ROI 2 is then applied as a logical "AND" operation and only the fibres that pass through both ROI's are retained.

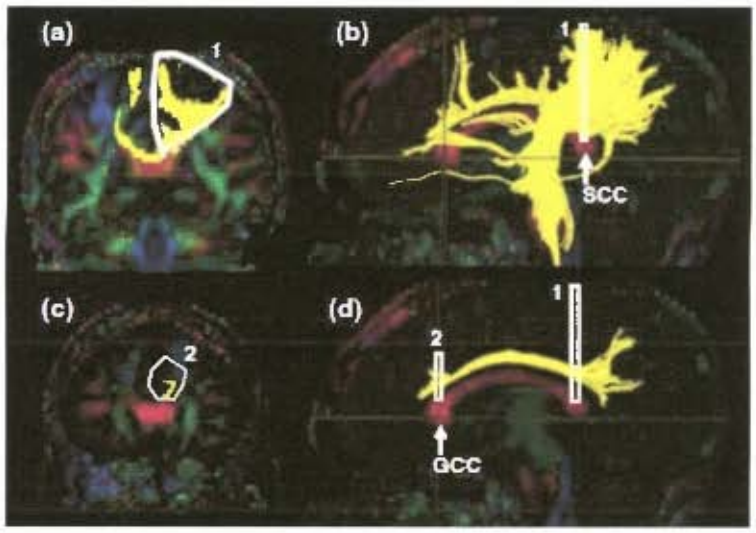

Figure 2.9: The landmark based two-ROI protocol for extracting the Cingulum Bundle (CB). In (a.) and (b.) ROI 1 is drawn in line with the splenium of the corpus callosum (SCC) from which fibre tracking is initiated. In (c.) and (d.), ROI 2 is drawn in line with the genu of the corpus callosum (GCC), and using an AND Boolean operation, the CB is isolated from the initial fibres which were tracked. Image from Wakana *et al.* (2007).

one-ROI approach, which generally results in an abundance of different fibre tracts which makes tract identification difficult.

2.2.3 Combining fMRI and DTI

Using fMRI to define seed ROI's is an intuitive step for initiating tractography. A fundamental problem that needs to be addressed when using this approach is that fMRI activations are limited to grey matter, whereas DTI is only reliably performed in white matter. Given that functional connectivity between localised brain regions can be observed using fMRI techniques, the circuitry which connects these areas should reflect the same network characteristics. In tractography, defining the seed points for a two-ROI approach is critical to the resulting tracts produced and usually relies on expert a priori anatomical knowledge. The use of DTI tractography has therefore been limited in discovering new connection patterns since it requires the prior knowledge and placement of ROI 1 to initiate the fibre tracking process. The definition of ROI 1 is the more critical and subjective aspect of the two-ROI method. In addition, if anatomical irregularities are present, such as in disease states or tumours, normal anatomical assumptions are no longer valid (Kim and Kim, 2005). If ROI 1 can be defined by fMRI activity then this initial requirement is automatically satisfied. Figure 2.10 describes the extraction of the Corticospinal Tract (CST) using this "modified two-ROI" approach.

University of Cape Town

Werring *et al.* (1999) were the first to combine fMRI and DTI. It was found that those regions with highest BOLD response corresponded with regions of tissue with lowest FA. Here, the fact that fMRI and DTI both use Echo Planar Imaging (EPI) is exploited by matching scanning parameters as closely as possible, thus ensuring that the geometric distortion artefacts are similar. Coregistration of the images was therefore not performed and fMRI regions were mapped directly onto FA maps.

Surgical planning and tumour location is an important application for combining fMRI and DTI (Clark *et al.*, 2003). Tractography is able to show how important nerve fibre tracts are diverted in the white matter and aid the neurosurgeon in devising an appropriate surgical

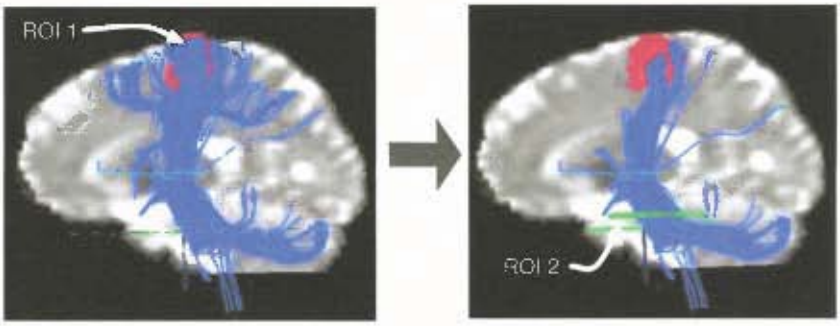

Figure 2.10: In a preliminary investigation, a fMRI activation in the motor cortex was used to define ROI 1 and a modified two-ROI approach was used to effectively extract the CST by applying a logical AND with ROI 2. Prior knowledge that the CST trajectory passes through the brain stem was required.

University of Cape Town

strategy. DTI and fMRI have been combined in surgical navigation studies (Kamada *et al.*, 2005; Smits *et al.*, 2007; Hattingen *et al.*, 2009), where tractography was initiated manually from seed regions "subadjacent" to maximal fMRI activation. Since tumours or disease states displace known anatomical structures, relying on atlas based information may result in poor tractography capability. The same limitation applies when conducting exploratory DTI tractography where the trajectories of the potential tracts of interest are not known.

In current surgical practice, functionally relevant brain areas are determined by direct electrical stimulation to the brain surface intraoperatively (Duffau *et al.*, 2003). Studies have shown that stimulation sites closely corresponded with DTI fibre tracts (Leclercq *et al.*, 2010; Smits *et al.*, 2007). The validity of combined fMRI/DTI has shown connectivity patterns that are highly specific and comparable to data obtained in macaques using well established neuroanatomical techniques based on post-mortem tracers (Dauguet *et al.*, 2006).

Greicius *et al.* (2009) used tractography to extract the white matter connections linking known components of the Default Mode Network (DMN). Similarly, van den Heuvel *et al.* (2009) extracted the structural connections of nine resting state fMRI networks. In both of these approaches, the fMRI ROIs were arbitrarily dilated to extend into the white matter (Greicius *et al.* (2009) by 3-4 mm and van den Heuvel *et al.* (2009) by 4 mm). As in previous

studies incorporating fMRI and DTI, these methods require manual intervention of the fMRI ROI's to effectively seed tractography (Mulkern *et al.*, 2006).

In an investigation into the structure and function of the DMN, van den Heuvel *et al.* (2008a) found a positive correlation between the level and functional connectivity and the FA measure of structural connectivity. The finding can be interpreted as evidence for the association between structural and functional connectivity. Although both fMRI and DTI are widely used, both provide indirect measurements and the interpretation may be elusive and difficult to quantify (Horwitz, 2003).

University of Cape Town

2.2.4 Relevant Neuroanatomy

White Matter Bundle Classes

Macroscopically, the white matter can be seen to form fibre collections known as tracts. Structural connectivity in the brain refers to the white matter tracts, which describe the millions of long distance axons that directly interconnect large groups of spatially separated neurons. Four main types of fibre tracts can be classified in the brain (Jellison *et al.*, 2004):

- Projection Fibres
  Connect the cerebral cortex to subcortical centres. These are either ascending or descending, e.g.. Corticospinal, corticopontine tracts, corona radiata, internal capsule, optic radiation.
- Short Association Fibres
  Connect adjacent gyri within one hemisphere; also known as "U"-fibres.
- Long Association Fibres
  Connect different cortical areas within one hemisphere with a range that extends beyond adjacent gyri, e.g. Cingulum Bundle, Superior Occipitofrontal Fasciculus, Inferior Occipitofrontal Fasciculus.

- Commisural Fibres
  Connect cortical areas between hemispheres of the brain, e.g. Corpus callosum, anterior commissure.

In white matter connectivity analyses, we are largely uninterested in the short association fibres ("U" fibres) as these represent local connectivity (DeFelipe *et al.*, 2010) and are typically much smaller than the other large fibre bundles. The focus in this thesis is on the long range connections between distant parts of the brain. The anatomically separate functional networks of the brain as described in relation to functional connectivity MRI (Section 2.2.1) are supported by specific white matter tracts (Greicius *et al.*, 2009). Although high functional connectivity is also observed between regions connected by short-range fibres, the long range connections between remote regions support functional integration by massively parallel brain networks, so that function emerges from the flow of information between distant brain areas supported by the long range-fibre tracts (Ramnani *et al.*, 2004).

University of Cape Town

Cortical Layers and Columns

In the grey matter of the cortex there is vertical and horizontal microstructural organisation. The neocortex is divided into six layers over its thickness of 2-4 mm. Each layer contains characteristic neurons with variations in cell type, density and size. The layers range from layer I (adjacent to the cortical surface) to layer VI (where the axons project into the white matter). The density of cells in the six layers of the cortex, and in three different brain regions, is illustrated in Figure 2.11. The layers of the cortex have distinct functional significance and the same cell type in different layers may have varying functional roles.

According to the minicolumn hypothesis (Buxhoeveden and Casanova, 2002), there is a strong tendency for the cortical cell types to extend their processes perpendicular to the cortical surface (vertically in Figure 2.11), forming distinct functional units, or minicolumns. The most striking structural component of this radially oriented minicolumn is the apical dendrite of the pyramidal cells. The size of the pyramidal cell is proportional to the distance the axon must travel. Therefore the pyramidal cells of the primary motor cortex are the most prominent, as is evident in Figure 2.11. The vertical, columnar organisation of the these

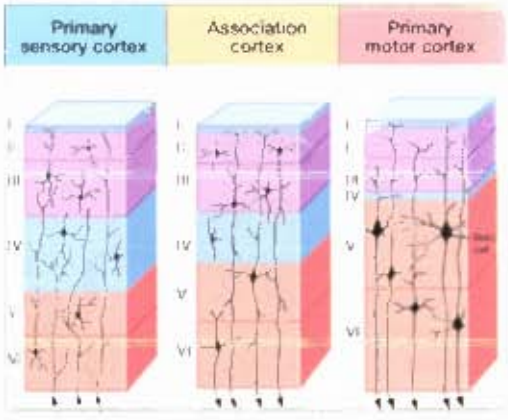

Figure 2.11: Cellular properties of three distinct grey matter regions. Axons enter or leave layer VI, while dendrites branch off within the grey matter interconnecting local neurons. The layers vary in thickness, as well as cellular structure. For example, the primary motor cortex is characterised by giant pyramidal neurons (Betz cells). Image from Joseph and Heckers (1996).

minicolumns is reflected not only in dendritic and axonal bundles, but also in the grouping of cell bodies into interconnected functional units of neurons (Buxhoeveden and Casanova, 2002). This arrangement is shown in Figures 2.12 and 2.13.

Cortical Development and Grey Matter Maturation

The sequence of prenatal and postnatal neural ontology during development hints at the underlying structure. Most cortical neurons migrate from near the cerebral ventricles towards the cortex along a radially arranged scaffolding of specialised glial cells called radial glia, arriving at the cortical destination and following a well-defined, radially oriented, columnar organisation (Rakic, 2003). This is shown in Figure 2.14, where the radial structure of the cerebral cortex is depicted. According to this radial unit hypothesis of cortical expansion, progenitor cells from subventricular zone migrate along radial glial cells forming radial extensions to the cortex. This has been largely accepted as a principle for understanding the formation of the cerebral cortex (Rakic, 2007) and is illustrated in Figure 2.14b. As cortical folding progresses after birth, the radial scaffolding guides the axons to their cortical destinations. They migrate towards the cortical plate from the intermediate zone which is the

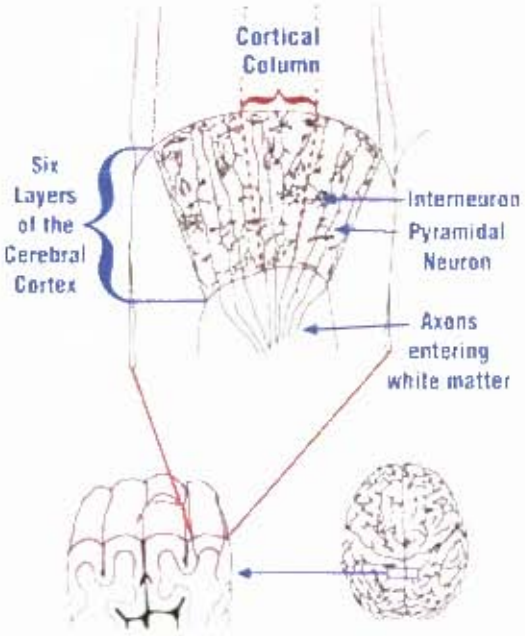

Figure 2.12: Cortical columns with axons entering the white matter. Image from Noback (2005).

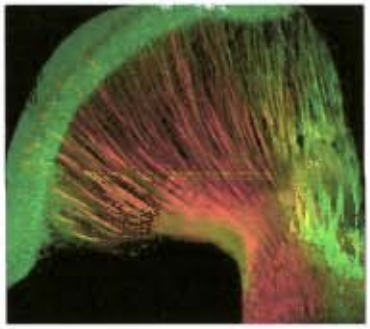

Figure 2.13: Radial structure in the frontal cortex (image from Joseph and Heckers (1996)). These images are produced by immunohistochemical staining with RC2 antibody (green) and anti-GABA (red).

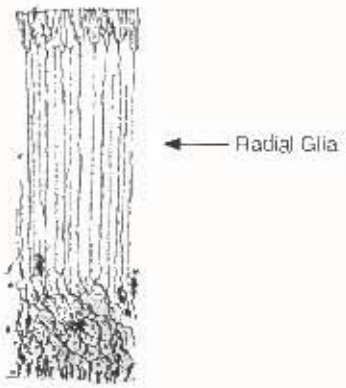

(a) Radial glia and neuroglia of the cerebral cortex in neonatal rabbit stained with the Golgi method. Image from Rakic (2003), adapted from Ramon y Cajal (1909).

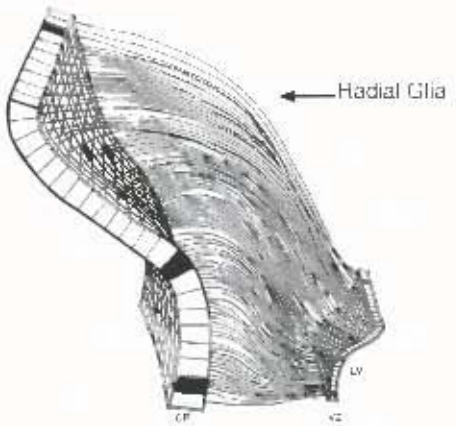

(b) A 3-D representation of the radial units hypothesis showing regular arrays of radial glial fibres stretching from the Ventricular Zone (VZ) adjacent to the Lateral Ventricle (LV) to the convoluted Cortical Plate (CP). The black squares highlight correspondence between the LV and CP. Image from Rakic (2003)

Figure 2.14: The radial glia of the cerebral cortex.

University of Cape Town

neuroembryological term for what is now the white matter of the brain. This radial structure is present into adulthood and is associated with constant rewiring and even neurogenesis which persists, though to a lesser degree than in childhood (Ghashghaei *et al.*, 2007). As the brain matures, the radial scaffolding becomes less prominent, and the axons and dendrites branch out tangentially to form locally interconnected circuits. As a result, the diffusion in the cortex becomes increasingly restricted in all directions. In mature human brains the radial organisation of the external cortical layers, with only the principal eigenvectors taken into account, is still observable (Menab *et al.*, 2009).

Myelination and neural pruning occur at a dramatic pace in the early postnatal period with the formation of new connections. Neural maturation involves elaboration of dendrites and axons, formation of interneurons, formation and regression of synaptic connections, and selective elimination of cell populations (pruning) (McKinstry *et al.*, 2002). Radial structures in the grey matter columns restrict water displacement parallel to the cortical surface more than orthogonal to it due to the tangential dendrites. On the other hand, interneurons confound this radial evidence in the DTI signal. The myelination of the cortex begins just after birth and continues to around age 18, but some parts of the brain are fully myelinated long

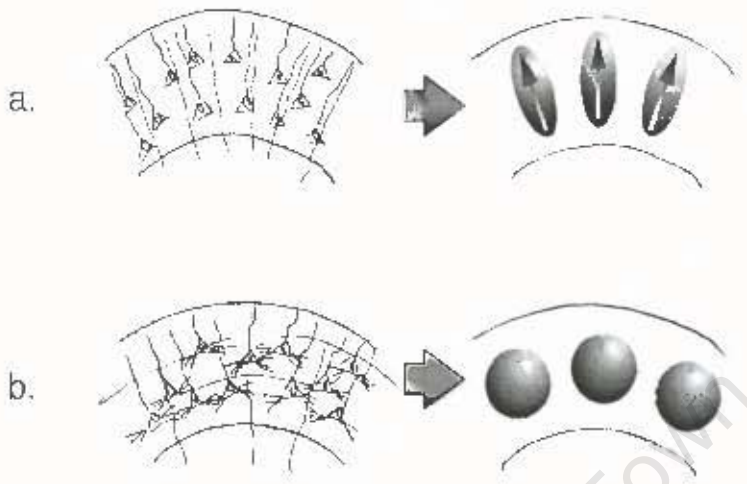

Figure 2.15: Development of cortical anisoptropy in pre-term human infants in the immature (a.) and mature (b.) cases. Tangential developments such as dendritic branching cause loss of radial anisotropy when taking the principal diffusion direction into account. Adapted from McKinstry *et al.* (2002).

University of Cape Town

before that. The cortical interneurons take a tangential path to reach the cortex and travel relatively long distances, whereas pyramidal cells take a predominantly radial path thereby reaching the cortex more directly. Since the tangential interneurons are not myelinated they would have less effect on the diffusion of water than the myelinated axons, therefore being less influential on the DTI signal. Anisotropy changes with increasing brain development reflects these microscopic developments (as illustrated in Figure 2.15), and it has also been noted that the change is greater in WM than in central GM (Mukherjee *et al.*, 2001). The change in GM properties is related to the change in anisotropy since axonal membranes and myelination, characteristic of the white matter, largely modulate diffusion characteristics (Beaulieu, 2002).

The Grey - White Matter Interface

DTI in grey matter is an ongoing area of research (Anwander *et al.*, 2009). Since partial volume effects confound the ability of DTI to delineate microstructure it is difficult to be certain of the path of fibres at the typical DTI resolution. The spatial resolution required to show both tissue types of the tissue boundary is significantly smaller than the typical DTI

voxel size of an isotropic 2-3 mm. However, since DTI is a T2 based MRI technique, a sharp contrast is observed between GM and WM, and this contrast originates from the interaction of water with the myelin sheath.

Fractional anisotropy maps provide excellent grey / white matter contrast for characterisation of evolving white matter (Kim *et al.*, 2007). Variable cortical anisotropy has been attributed to the relative abundance of large pyramidal neurons, as observed by Anwander *et al.* (2009) in the motor cortex, but has not been investigated in other regions.

The diffusion tensor signal has been related to this cortical grey matter structure in animals (Ronen *et al.*, 2003), in the human fetal cerebrum (McKinstry *et al.*, 2002) and also in the adult human brain (Tuch *et al.*, 2003b). In the adult brain this was done using a more complex model of diffusion than the simple tensor model (see subsection 2.2.2). Using Q-ball imaging, the diffusion component oriented perpendicular to the cortical surface could be resolved (Tuch *et al.*, 2003b).

Ultrahigh-resolution DTI has been performed by Jaermann *et al.* (2008) who, at a resolution of 0.58×0.58 mm^2, were able to show the termination of fibre trajectories in the cortical grey matter. Yassa *et al.* (2010) were also able to achieve sub-millimetre resolution (0.6 mm isometric) in order to investigate the specific microstructural detail of the perforant path, a white matter pathway in the medial temporal lobe which links to the hippocampus. By varying the b-values of Equation 2.1, Ronen *et al.* (2003) and by looking at the component which was sensitive to the slow diffusion characteristics, they could follow the radial fibres into the grey matter.

The diffusion signal component normal to the surface could be due to radially projecting axons or radially oriented grey matter minicolumns. As the white matter fibres insert into the cortex, the diffusion signal is predominantly oriented radially to the surface. A schematic of this is shown in Figure 2.16. The fibres bend rapidly as they are taken up by the white matter core and this curvature cannot be resolved by conventional tractography However, once on the central white matter, tractography can be implemented.

University of Cape Town

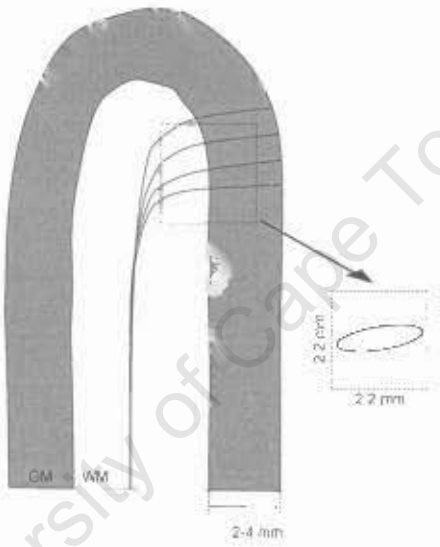

Figure 2.16: Schematic of white matter insertion into the grey matter. The arch represents a gyrus with fibres extending into the cortex. The resolution of a typical DTI voxel is shown in relation to the approximate thickness of the grey matter. The diffusion ellipsoid aligned normal to the surface arises from radially oriented fibres and radial grey matter architecture also contributes. This pixel is illustrates a typical DTI voxel. Adapted from Tuch *et al.* (2003b).

University of Cape Town

Neuronal activity in a grey matter region area may be dependent on how well the action potential is transported along the axons, and thus on local fibre microstructure in the white matter immediately subjacent to it. Thus regions with high BOLD response may have higher radiality associated with them (DeFelipe *et al.*, 2010).

The Corticospinal Tract

The motor system is one of the most widely studied and best understood systems related to brain function. For this reason it is a useful candidate for validation of DTI tractography. The major motor pathway, the corticospinal tract (CST) is a projection fibre system which starts in the primary motor cortex (M1) and ends in the spine, passing through the brain-stem. The basic somatotopic arrangement of the motor cortex is depicted in the popular homunculus of Penfield (Penfield, 1950) (reproduced in Figure 2.17). As stated above, the majority of fibres making up the CST originate in M1, located in the pre-central gyrus. However, other cortical and subcortical areas contribute as well. For example, the supplementary motor area and motor areas of the frontal lobe cortex also send projections to the CST (Kollias *et al.*, 2001). The CST is also known as the pyramidal tract because M1 contains large pyramidal neurons, from which the axons of the CST originate, and also because it passes through the pyramids of the brain stem.

University of Cape Town

M1 is not the only area of the brain to contain pyramidal cells, but it has especially large pyramidal neurons called Betz cells (up to 120μm). In general the longer the distance that the axon must travel, the larger the pyramidal neuron. Betz cells contribute only 3% of the fibres of the pyramidal tract. The remainder of the CST is made up of fibres from other layer V pyramidal cells. The increased diversity in pyramidal cell sizes suggests the multitude of destinations for its efferent fibres.

The axons leave the pyramidal neurons and enter the white matter just below layer VI. Each gyrus has a central core of white matter, which contains all of the axons entering or leaving the gyrus, and these axons are then taken up by the major fibre tracts as they enter the deep WM. In the case of the CST, it forms part of the corona radiata which then becomes the internal capsule as it enters the deep nuclei of the brain. The descending axons then travel

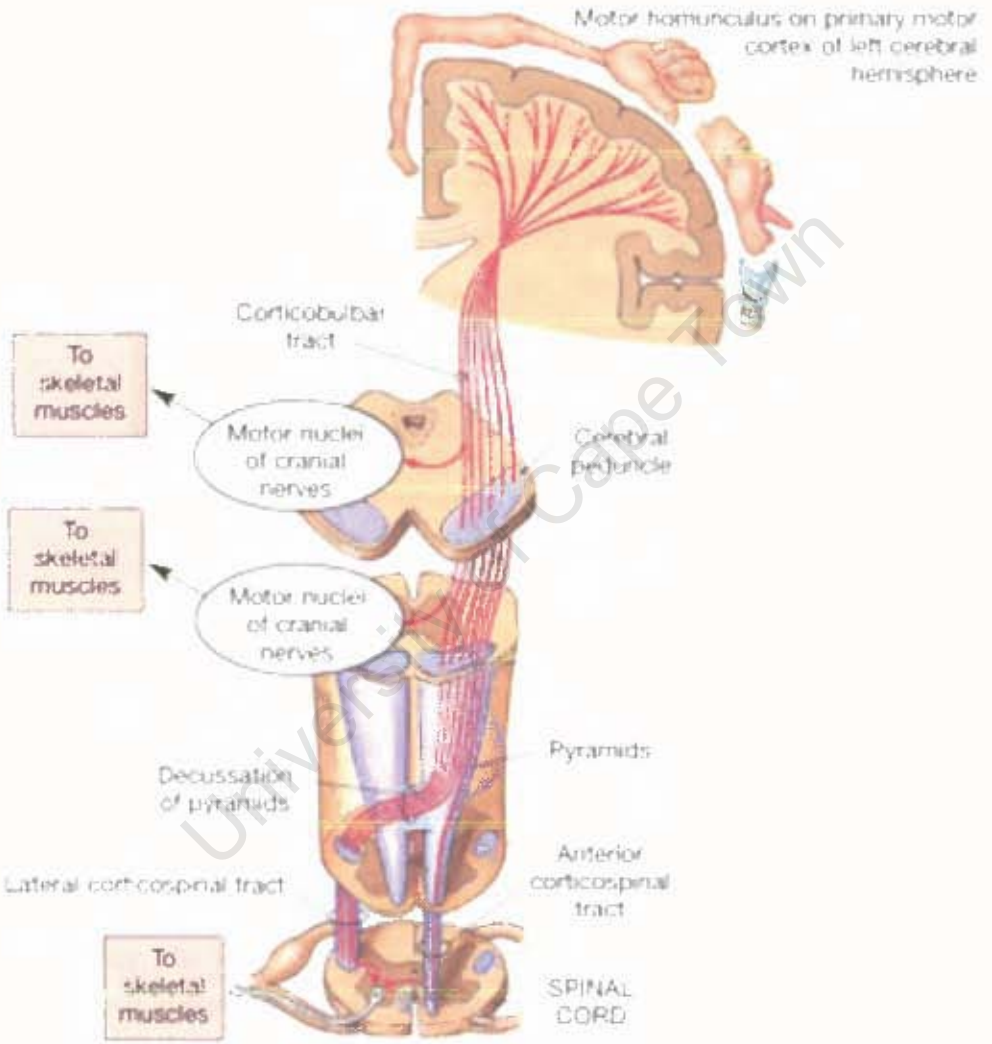

Figure 2.17: The pathway of the descending corticospinal tracts relative to the homunculus of the motor cortex in the pre-central gyrus. Image from Joseph and Heckers (1996).

University of Cape Town

Figure 2.18: Tractography results showing the corticospinal tract. The blue arrow indicates the region where the tract diverges to the callosal motor fibres that connect the primary motor cortices (M1) of the two hemispheres.

University of Cape Town

through the posterior limb of the internal capsule through the cerebral peduncles. Once the axons reach the level of the pons, some of the fibres veer off via the cerebellar peduncles to the cerebellum. The remaining fibres pass through the pyramids of the medulla where decussation occurs and they go onto the spinal cord (Johansen-Berg, 2001). The course of the CST is shown in Figure 2.17.

Using tractography, the CST path is reproduced in Figure 2.18. In addition to the main pathways described above, tractography reproduces the callosal motor fibres which connect the M1 regions of the two hemispheres.

The Cingulum Bundle

The Cingulum Bundle (CB) is a large white matter tract which has been shown to connect the frontal and parietal sites of the Default Mode Network (DMN). The existence of direct structural white matter pathways between the regions of the DMN has been demonstrated by Greicius *et al.* (2009), who suggest an important role for the CB in connecting the DMN mid-line structures, the mPFC (medial Prefrontal Cortex) and the Posterior Cingulate Cortex (PCC). The efficiency of the DMN may depend largely on the integrity of this important tract. Another DTI study showed a direct association between the level of functional activity of the DMN and the level of microstructural organisation of the CB (van den Heuvel *et al.*, 2008a). In addition, Greicius *et al.* (2009) recommended extending their investigation to combine structural and functional approaches in the same subjects, because it would allow for superior characterisation of DMN changes caused by disease. Connections between other nodes of the DMN are not as robust and are subject to crossing fibres in those regions (Mori and Zhang, 2006). In fcMRI a reduced functional connectivity between the PCC and mPFC has been demonstrated in Assaf *et al.* (2010), which indicates that investigation of the anatomical basis for the DMN could be represented in the CB. These findings suggests that the DMN operates as a single unit so that the connectivity of its nodes, and in particular the CB, can serve as a proxy for the connectivity within the entire network (Teipel *et al.*, 2010). The CB is composed of long association fibres.

University of Cape Town

2.3 Methods

2.3.1 Data Acquisition

The subjects were all females drawn from the same population group with no physical illness or psychopathology. Eleven age, sex, education and IQ matched subjects were included in the study. All subjects gave informed consent and the study was approved by the University of Cape Town Institutional Review Board.

All MRI scans were performed on a 3T Siemens (Erlangen, Germany) MAGNETOM Allegra

syngo MR 2004A brain scanner at CUBIC (Cape Universities Brain Imaging Centre) using a four channel head-coil.

Unless otherwise stated, all processing was performed in Matlab^{TM} (MathWorks, Natick, MA).

fMRI acquisition

A finger tapping motor task was performed using an on-off block paradigm with five 30 second epochs of task interspersed with five 30 second rest periods. During the task periods, the subjects were visually prompted to tap each of the fingers successively against the thumb on both hands simultaneously. An Echo Planar Imaging (EPI) sequence was used with parameters: TR = 2000 ms; TE = 27 ms; flip angle 70°; voxel size 3.5 × 3.5 × 3.5 mm^3, 36 slices covering whole brain.

In the same scanning session, each subject underwent a resting state scan. Subjects were scanned using an EPI sequence for a period of five minutes, with the instruction to close their eyes and relax, in accordance with similar studies in the literature (Greicius *et al.*, 2003; Zhou *et al.*, 2008; van den Heuvel *et al.*, 2008b). BOLD data were acquired using scan parameters identical to those used for the motor task.

University of Cape Town

DTI Acquisition

Six non-diffusion weighted ($b = 0$) and 30 diffusion weighted datasets were captured in 30 gradient directions with a b value of 1000 s/mm^2. Scan parameters were TR = 9000 ms, TE = 88ms, FOV = 260 mm with a matrix size of 120 x 120 and a slice thickness of 2.2 mm.

The DTI data were acquired in accordance with the methods prescribed in Andersson *et al.* (2003) which is specifically designed to minimise susceptibility artefacts. Two EPI images were acquired with reversed phase encoding directions to allow for later artefact reduction

in post-processing, as described in Section 2.3.3.

Structural MRI Acquisition

Each subject also underwent a T1 weighted high resolution Magnetization Prepared Rapid Gradient Echo (MP-RAGE) structural scan. The MP-RAGE parameters were: TR=2300 ms; TE=3.93 ms; Flip angle=9°; inversion time (TI)=1100 ms; delay time (TD)=200 ms; matrix=256×256; FoV=256 mm; voxel size = 1×1×1 mm^3.

2.3.2 fMRI Processing

The fMRI data were processed using SPM (Statistical Parametric Mapping, version 5) (`http://www.fil.ion.ucl.ac.uk/spm/`) which is a widely used tool in the neuroscience community. Motion correction was performed in SPM, the images were initially realigned using a six parameter (rigid body) model to determine the transformation parameters needed to align all of the BOLD images to the first image in the series, using a least squares comparison. A report which reflects the subject motion in the scanner was generated, and based on this, two fMRI datasets had to be discarded due to motion greater than 1 mm. The data were then smoothed using a 6 × 6 × 6 mm^3 Gaussian kernel.

University of Cape Town

Motor Cortex

An experimental design matrix was set up in accordance with the protocol described in Section 2.3.1. The Canonical HRF setting was used to interpret the data.

Default Mode Network

The functional connectivity analysis was performed using GIFT (Group ICA Functional Toolbox) (`http://icatb.sourceforge.net/`, version 2.0b), which is a Matlab toolbox that

works with SPM (Calhoun *et al.*, 2001). The first five volumes were discarded to allow for signal equilibration effects. The number of independent components was set to 20 and the Infomax (Bell and Sejnowski, 1995) ICA algorithm was applied using the default settings. The GIFT ICA analysis was performed for each subject individually. While GIFT is capable of performing ICA on multiple subjects, it is also possible to perform single subject analyses, in which case there is a single data reduction step and group statistics cannot be calculated. The DMN activation pattern was identified in all subjects based on visual inspection.

fMRI Thresholding

The first step in analysing the output of an fMRI analysis is to define a statistical threshold (using t-statistic or Z-score maps). The output image is scaled to a p-value, upon which a threshold is imposed. For example, if the value of Z is greater than 2.58, then there is a 99.5% chance that the null hypothesis (that the activation is not due to the associated task) is false. This corresponds to a p-value of $p = 0.005$, which depends on a normal distribution. This thresholded image can be overlaid on a high resolution structural brain image in order to identify the anatomical regions in which pixels are "activated" to this level of confidence.

University of Cape Town

However, for the purposes of this project, the statistical significance of the activation is not paramount. For the same task, the level of activity will vary between subjects, depending on task compliance, subject motion, image noise, and other factors. However, for this application it is essential that the spatial extent of grey matter activation is similar across subjects, regardless of noise. Also, when considering the individual variation of this task, a group analysis is not possible since inappropriate seed placement may lead to spurious tracking results. A large individual variation was evident in all initial fMRI exploratory analyses using the standard Family Wise Error (FWE), False Discovery Rate (FDR) or uncorrected, voxel level p-value thresholding. SPM multivariate analyses impose strict limitations on the statistical significance of activations. This resulted in low spatial extent of activity in some subjects, as shown in Figure 2.19 using a fixed threshold of $Z > 1.6$.

An alternative to the null hypothesis testing is a technique called mixture modelling which

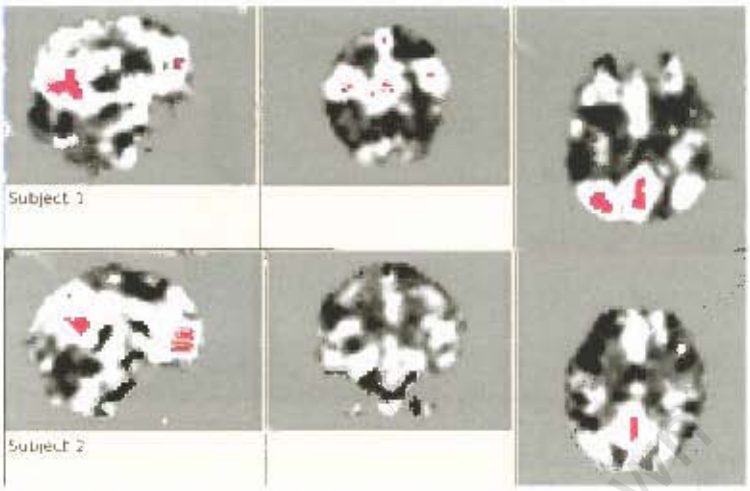

Figure 2.19: Z-score thresholding produced low spatial extent in the DMN for a threshold of Z >1.6 in these two subjects.

University of Cape Town

was employed in order to standardise the thresholding step (Woolrich *et al.*, 2004). A mixture of distributions are fitted to the intensity histogram of the statistic of interest resulting in relatively large activation clusters. The most significant advantage of the mixture modelling is that inference can be carried out on the statistical maps output from the fMRI analysis and regions of brain activity can be determined completely objectively (Smith *et al.*, 2005).

The result of mixture modelling is a map of the probability of the particular region lying in each of the segmentation classes (null, activation and deactivation). The spatial regularisation is determined adaptively from the data using a spatial Markov random field to regularise the labelling of voxels. The curve fitting and regularisation does not have to be tuned heuristically, but is adaptively extracted from the data. The curve fitting using intensity histograms automatically scales to the data (as shown in Figure 2.20), therefore a consistent threshold can be applied to the probability output images since all parameters in the model are adaptively determined. Figure 2.21 shows an example probability map after mixture modelling has been applied.

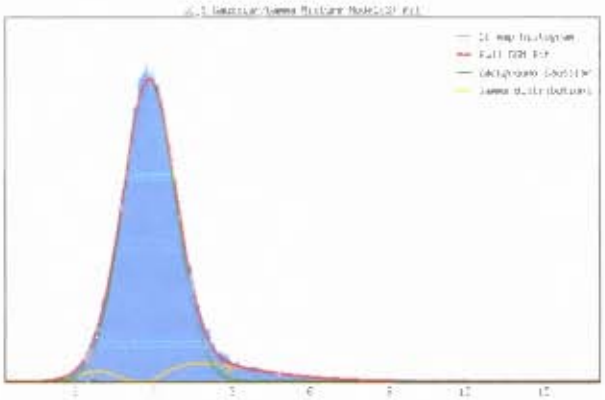

Figure 2.20: A mixture model fit is performed on the histogram of the Z-statistic image. In our case we are interested in the activation class which is determined by a gamma distribution (yellow curve). A Gaussian curve (red) represents the central non-activation part of the data.

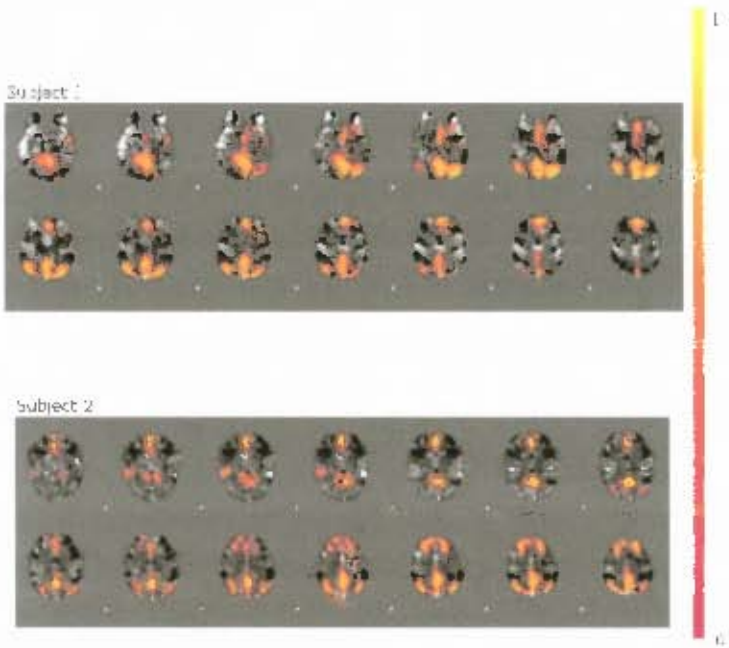

Figure 2.21: A probability map based on a mixture model fit of the activation class results in robust and consistent extraction of the Default Mode Network. DMN activation patterns for subjects a. and b. have been achieved using mixture modelling. The resulting probability threshold (rather than a p-value threshold) is set at P=0.5, with the colour bar ranging from zero to one.

2.3.3 DTI Processing

Distortion Artefact Reduction

The diffusion tensor data are acquired as a series of diffusion weighted EPI images with different diffusion gradients applied. One of the problems with EPI is the geometrical distortions in the resulting images caused by magnetic field inhomogeneities, especially near junctions of tissues with differing magnetic susceptibility (susceptibility artefacts) for example, in the frontal lobes which are near the nasal sinuses. Artefacts are introduced by the rapid switching of gradient directions (eddy current artefacts). These effects manifest as image distortions and a displacement of anatomical structures. Subject motion can also affect the resulting image quality, which causes misregistration among the diffusion weighted images and resulting errors in the derivation of the diffusion tensor. This results in faults in the fibre tracking and derivation of diffusion measures such as the FA and MD maps. Susceptibility artefacts and eddy current artefacts were minimised in preprocessing steps prior to deriving the diffusion tensor.

Based on the methods set out in Andersson *et al.* (2003), the DTI EPI images were acquired in pairs with alternately reversed phase encoding directions, one top down (anterior-posterior) and the other bottom up (posterior-anterior). The resulting susceptibility distortions in the images are then equal and opposite in magnitude. The distortion field was estimated using non-diffusion weighted images (b=0, b0) and this distortion field was then used to correct the diffusion weighted images. Six b0 images were acquired for each scan and these were averaged in order to improve the Signal to Noise Ratio (SNR) of the b0 image. This distortion field was then applied in opposite directions to the entire series of diffusion weighted images (Andersson *et al.*, 2003). Eddy current and simple head motion were then corrected for using an affine registration of the diffusion weighted volumes to the b0 volume.

Outlier Rejection and Averaging

Outlier diffusion signals are evident as large, unpredictable signal variations after calculating the diffusion tensors. Outliers were rejected by first calculating Z-scores based on 25 and 75

University of Cape Town

percentile limits, and then discarding data points more than 3 standard deviations beyond the mean. The discarded data points were recovered from the other dataset in the process. The two datasets were then averaged to produce a single, corrected DTI dataset per subject.

Software from the Oxford Centre for Functional MRI of the Brain (FMRIB) was used for DTI processing. The FSL (FMRIB's Software Library, version 4.1) software suite was then used for the processing and analysis of diffusion weighted images in order to calculate the diffusion tensor, eigenvectors, eigenvalues and scalar diffusion maps (including FA and MD).

University of Cape Town

2.3.4 Combining fMRI and DTI using Region Growing

The platform used for the algorithm development was mrDiffusion, which is a neuroimaging package developed and used by Stanford University Department of Psychology. This package is Matlab based and the code for the algorithms developed in this section were incorporated into the mrDiffusion platform. This package is freely available for download (`http://white.stanford.edu/software/`), licensed under the Gnu Public License.

Intermodality Coregistration

The preprocessing of fMRI and DTI was conducted in each modality's native space since the analysis is done on a subject by subject basis. In order for fMRI regions to be used as DTI seeds, accurate registration is essential. Errors due to poor registration would result in the seed regions being incorrectly placed. Due to the fact that only intrasubject registration is required, the standard affine coregistration as implemented in SPM5 was expected to be sufficient.

The mean functional image is coregistered to each subject's b = 0 diffusion weighted image using a 12 degree-of-freedom affine transform, following this, the resulting spatial transformation parameters are determined and then applied to the binarised fMRI activations, this is depicted in Figure 2.22.

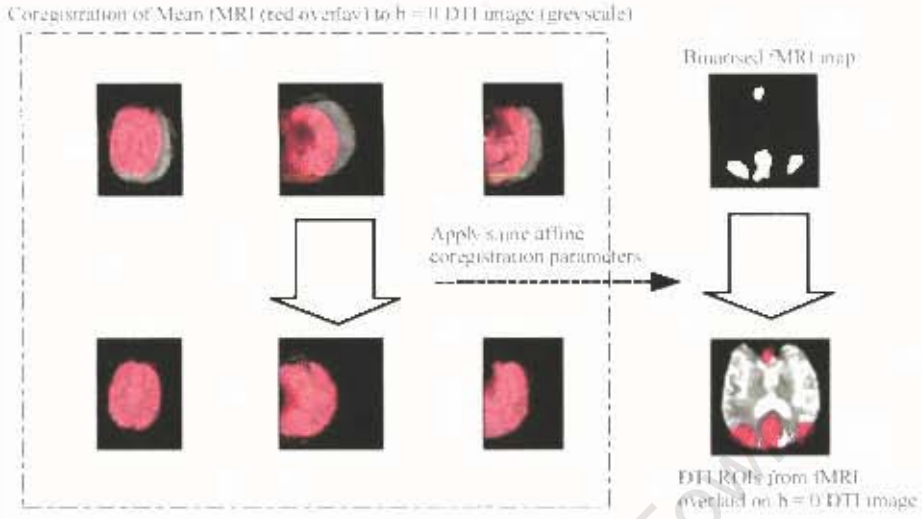

Figure 2.22: A summary of the intermodality coregistration procedure is shown. The fMRI image undergoes an affine transformation to match the DTI b0 image. The initially poor overlap is evident in the top three axial, coronal and sagittal views. The identical affine parameters were applied to the binarised fMRI activity map.

Calculation of White Matter Probability Images

The white matter surface was estimated using information from the diffusion tensor data. FA provides good GM/WM contrast, however this can be improved upon by calculating a white matter probability map, as implemented by mrDiffusion. White matter probability was calculated as a final probability score based on combined information from the b0 image, an FA error term and a MD error term. A target FA of between 0.25 and 1, and target MD of between 0.4 and 1×10^{-3}mm^2/s, were used to compute their error terms.

The b0 error is a z-score clipped at 4 standard deviations and normalised to the 0-1 range, since the intensity scale is arbitrary. The b0 image allows a specificity against artefacts in certain tissues such as sinuses which create very low b0 values but high FA and normal tissue ranges for MD. The overall white matter probability score is given as:

$$P_{WM} = (1 - \mathrm{err}_{\mathrm{FA}}) \times (1 - \mathrm{err}_{\mathrm{MD}}) \times (1 - \mathrm{err}_{\mathrm{b0}}) \tag{2.5}$$

University of Cape Town

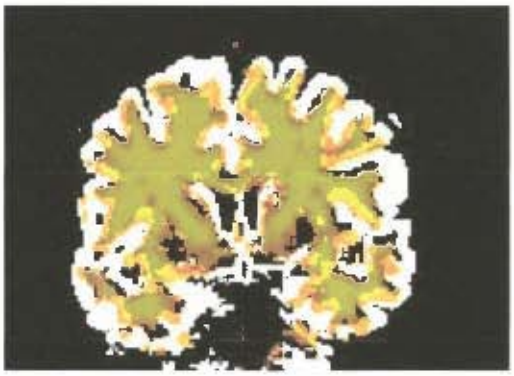

Figure 2.23: A white matter probability map (yellow) overlaid on an affine coregistered GM segmentation from a structural MRI scan in a pilot study shows misregistration errors.

A grey matter segmentation from a 3D T1 weighed structural image was considered as means to confine the fMRI activation to the grey matter. However, coregistering the structural image to the fMRI image resulted in obvious gyral/sulcal misalignment. A slice from one such coregistration is illustrated in Figure 2.23, where these errors are clearly apparent. fMRI and DTI produces similar images more suitable for coregistration as they are both EPI sequences with comparable image dimensions (Werring *et al.*, 1999). As a result, the T1 structural images were not incorporated in this study.

University of Cape Town

Calculation of a Radiality Metric

Radiality is defined here as the degree that white matter diffusion tensors line up with a vector normal to the grey/white matter boundary. First the white matter surface was defined using the white matter probability image which was first smoothed with a $3 \times 3 \times 3$ mm^3 Gaussian filter. A surface normal, termed the gradient vector, was then defined by taking the gradient across the white matter boundary. The radial orientation of the PDD's at the white matter boundary is clearly visible in Figure 2.24. The gradient vector is also defined for voxels close to the GM/WM interface since the WM probability image is first smoothed with a Gaussian filter.

A metric describing the alignment of the gradient vector with the entire tensor is required

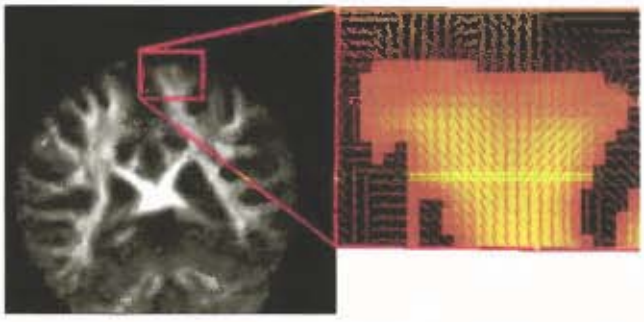

Figure 2.24: FA map with detail showing the PDD vectors (red) in relation to the white matter probability (orange).

to represent the degree of radiality with which the axonal tracts project into the white matter. The dot product between two vectors is a well known tool in vector algebra. It is also known as the scalar product. However, when dealing with tensors, there are a multitude of possible multiplication options (James *et al.*, 1999). Note that the product of a tensor and a vector is a vector, so we define the product of a vector with a tensor as the normalised sum of the gradient vector multiplied by each of the three eigenvectors of the diffusion tensor, weighted by the respective eigenvalues. This results in a scalar measure of the vector tensor product. Radiality can then be defined as the following normalised tensor vector product:

$$\text{Radiality} = \frac{(|\lambda_1||\underline{g}\cdot\underline{e}_1| - |\lambda_2||\underline{g}\cdot\underline{e}_2| + |\lambda_3|\,\underline{g}\cdot\underline{e}_3|)}{(|\lambda_1| + |\lambda_2| + |\lambda_3|) \times \underline{g}|} \tag{2.6}$$

Where $\underline{g}$ is the gradient vector, $\underline{e}_1$, $\underline{e}_2$ and $\underline{e}_3$ are the 3 eigenvectors of the tensor $\underline{\underline{D}}$ and λ_1, λ_2 and λ_3 are the respective eigenvalues. Rather than just the first eigenvector or principal diffusion direction, radiality is represented by all three eigenvectors and quantifies the degree to which the gradient vector lines up with the diffusion ellipsoid. Values range from 0 to 1, where 0 is the case where the tensor is tangential to the gradient and 1 corresponds to the tensor lining up perfectly with the gradient vector.

University of Cape Town

Radiality Based Fibre Tracking: The Modified two-ROI with RAFF Method

In conventional anatomy based DTI tractography, seeds are placed directly in the white matter. However, since the ROIs from fMRI lie mostly in the grey matter, the seed must be grown into the boundary region which is characterised by high radiality. Based on the evidence presented in Section 2.2.4, this method presumes that the grey / white matter interface is predominantly normal to the WM tracts arriving at the GM layers. This is largely due to the large axons descending from the radial cortical minicolumns. A boundary segmentation technique was implemented in order to efficiently seed the tractography.

Flood-fill algorithms are fundamental to image processing. They operate by starting from an original ROI and, searching all voxels exterior to and immediately adjacent to the ROI, the algorithm recursively finds the highest radiality voxels within a predefined radius and adds them to the original ROI.

A 3-D flood-fill algorithm was implemented for the task of segmenting regions characterised by high radiality at the GM/WM boundary. In this implementation, the flood-fill is initiated with a set of discrete points originally confined to the GM. Each point, with coordinates x, y and z is defined by its neighbouring voxels. For a six neighbour configuration, the edge connected neighbour voxels are defined as (x + 1, y, z), (x - 1, y, z), (x, y+ 1, z), (x, y - 1, z), (x, y, z+ 1) and (x, y, z - 1). A radiality threshold and a radius limitation was imposed to decide whether or not the voxel is to be included. The radius limit was set to three voxels ($\pm$7 mm). The three voxel limit was chosen in order to ensure that the tractograpy was robust, after initial attempts with one and two voxel limits yielded inconsistent results.

The flood-fill algorithm is similar in principle to the Fast Marching (FM) tractography algorithm as introduced in Section 2.2.2 in that a regional property determines the segmentation of the area, but it is not as sensitive to boundary detection as FM. The flood-fill approach, while less numerically precise than more advanced region based methods, enables the initial fMRI seed region to grow into the white matter where tracts are more likely to originate.

University of Cape Town

The algorithm for Radiality Flood-Fill (RAFF) proceeds as follows:

i. A metric describing the radiality of each voxel is calculated using Equation 2.6.

ii. The initial seed voxels are defined by the fMRI ROI constrained to the grey matter.

iii. The voxel with the highest radiality in the ROI is selected as the starting point and added to the solution matrix.

iv. The six voxels adjacent to the starting point are placed in a corresponding index matrix which keeps track of voxels which have been evaluated.

v. The voxel in the index matrix with the highest radiality is tested against a predefined radiality threshold and radius limit of less than three voxels from the border of the original ROI. If it meets these criteria this voxel is removed from the index matrix and added to the solution matrix. If it does not meet the criteria, then it is removed from the index matrix but *not* added to the solution matrix.

vi. A new neighbourhood of six voxels is defined around the new highest radiality voxel by adding them to the index matrix.

vii. Repeat steps v. and vi. until the index matrix is empty.

The preprocessed DTI data were loaded into the mrDiffusion program for fibre tracking to be performed. Within this toolbox, functions were developed or modified in order to directly import and manipulate fMRI ROIs as seed points. The fMRI ROIs were ordered by size, from largest to smallest. The largest two ROIs from the DMN activation were consistently the mid-line structures characterising the DMN, the mPFC and the PCC, as shown in Figure 2.25.

For comparative purposes, the landmark based two-ROI method was used to extract the CST and the CB. Polygonal ROIs were drawn directly on colour-coded FA maps in accordance with the two-ROI protocol defined for those specific tracts by Wakana *et al.* (2007). For the CB, ROI 1 was drawn in the coronal plane, in line with the splenium of the Corpus Callosum and ROI 2, in line with the genu. Similarly, the CST was extracted by placing ROI 1 as a polygon in the axial slice over the cerebral peduncle in line with the decussation of the superior cerebellar peduncle. Tracking was performed from ROI 1 and from the resulting fibres,

University of Cape Town

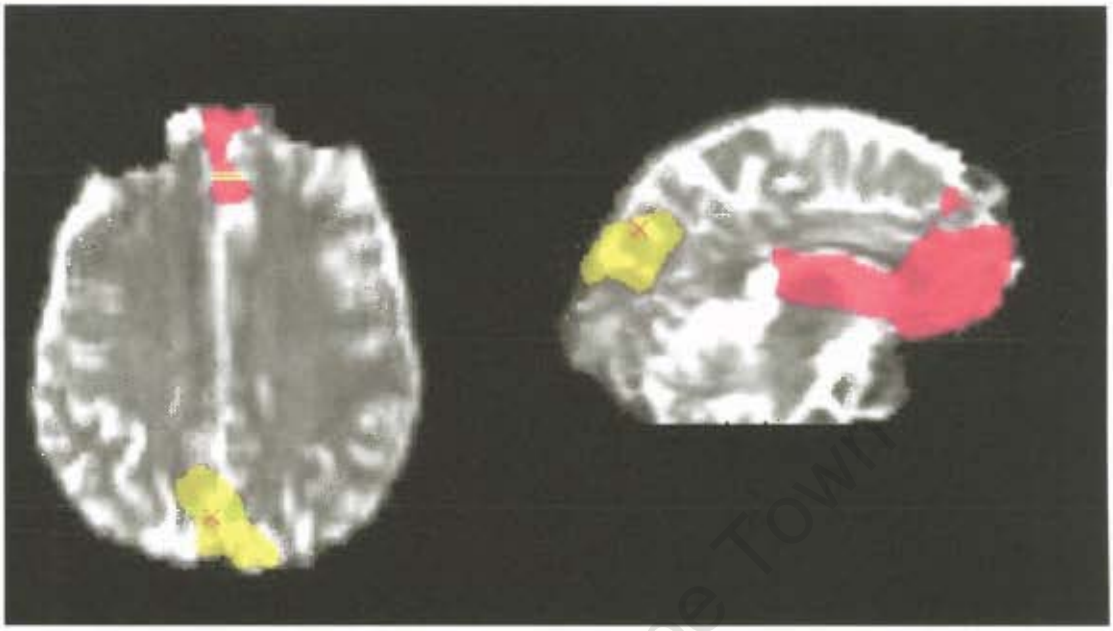

Figure 2.25: The largest activated ROIs are imported into the fibre tracking program. Here the cortical mid-line structures of the DMN, the medial Prefrontal Cortex (mPFC) in red and the Posterior Cingulate Cortex (PCC) in yellow.

the trajectory of the CST is identified on a higher axial slice in right after the bifurcation to the motor and sensory cortex. The libres going towards the central sulcus (CS) and the projection to the motor cortex were identified and the CST was selected. The two-ROI with RAFF method for the CB is depicted in Figure 2.26.

The tractography steps and parameters for a modified two-ROI with RAFF method can be summarised as follows:

i. Binarised ROI masks were loaded into mrDiffusion.

ii. In order to ensure that the seed was initiated in the grey matter, it was confined to the grey matter using the white matter probability. The white matter probability was set at 0.6.

iii. The ROI was extended into the white matter using RAFF. Parameter settings: radiality – 0.5; radius limit – 3 voxels (+7 mm).

iv. Tractography was performed using the FACT algorithm. In each voxel, 9 seeds were

University of Cape Town

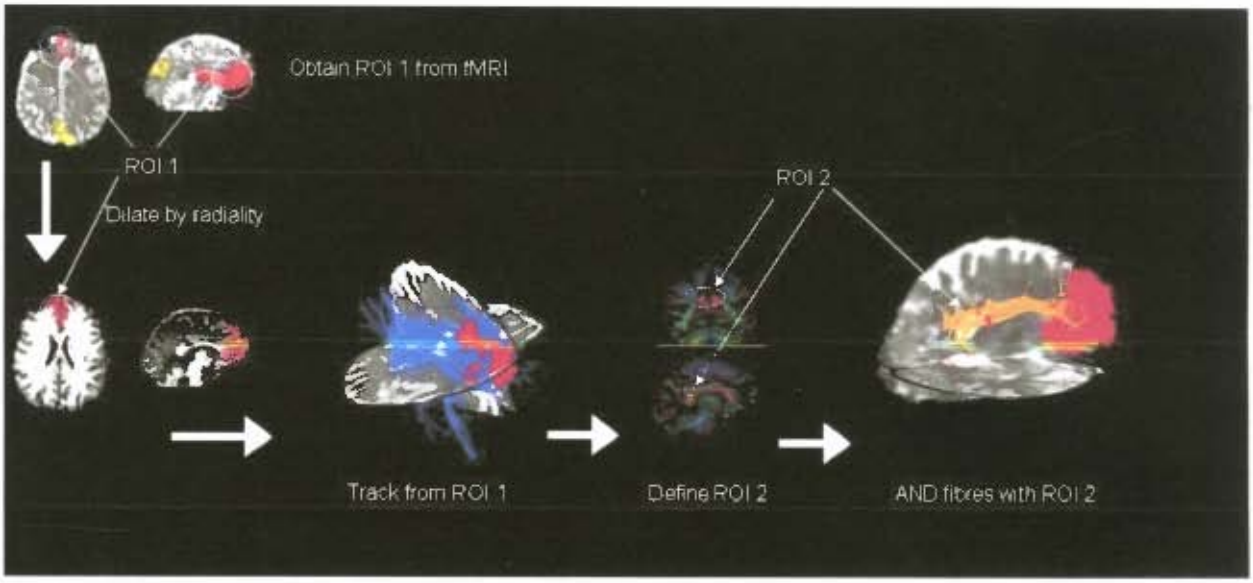

Figure 2.26: The Cingulum Bundle was extracted in each individual subject using a modified two-ROI with RAFF method. ROI 1 was dilated with the radiality metric before being selected with ROI 2 based on the known path of the CB.

started using a step size of 1 mm. Tracking was stopped when the fibre encountered a voxel with an FA value < 0.1 or when it had an average angle change between the neighbouring eigenvectors of $> 30°$. Only fibres with a minimum length of 50 mm were kept.

v. Define ROI 2 using anatomical landmarks.

vi. A Boolean AND operation selects only those fibres passing through ROI 2.

2.3.5 Validation Using Cohen's Kappa

Cohen's kappa is an established statistical measure of agreement for comparing inter and intra-rater reproducibility of qualitative measurement techniques, which considers agreement beyond that expected by chance (Landis and Koch, 1977). The kappa method has been applied to DTI protocols in various studies in order to quantify the inter and intra-rater validity of the tracts produced by the two-ROI method (Wakana *et al.*, 2007; Ozturk *et al.*, 2008; Zhang *et al.*, 2008; Voineskos *et al.*, 2009).

Cohen's kappa is used here to measure agreement between the tracts derived from the modified two-ROI method with RAFF and the corresponding tracts derived from the standard purely landmark based two-ROI method. As a further validation step, the performance of the RAFF was evaluated against a uniform morphological dilation of the equivalent three voxels from the fMRI ROI. The tracts derived from the uniformly dilated ROI were also compared to the landmark based two-ROI method. This validation strategy is described in Figure 2.27.

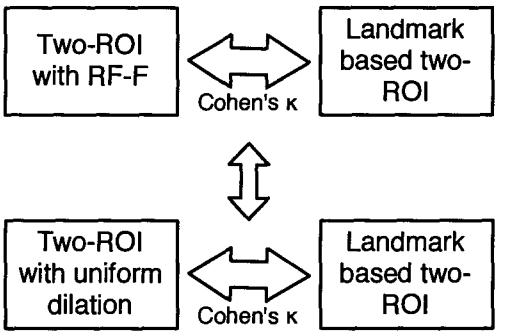

Figure 2.27: Validation strategy for comparing the radiality flood-fill approach to previously established fibre tracking methods.

To derive a kappa statistic for each pair of tracts, the tracking results for both the landmark based two-ROI and the modified two-ROI from fMRI methods were first converted to binary information at the same resolution as the DTI data (120 × 120× 65). Each pixel occupied by a tract was assigned a value of 1 and non-occupied pixels, a value of 0. By superimposing two tracking results, four pixel categories were obtained:

i. pixels not containing the tract in both cases (nn)

ii. pixels that contained the tract in only one of the tracts (pn or np)

iii. pixels that contained the tracts in both cases (pp)

Expectation values for each class were calculated as:

$$\begin{aligned} &\text{Expected nn} \quad Enn = (nn+np)(nn+pn)/N \\ &\text{Expected np} \quad Enp = (nn+np)(np+pp)/N \\ &\text{Expected pn} \quad Epn = (nn+pn)(pn+pp)/N \\ &\text{Expected pp} \quad Epp = (pn+pp)(np+pp)/N \end{aligned} \tag{2.7}$$

where $N = nn+np+pn+pp$ is the total number of pixels per tract. κ (kappa) was calculated by:

$$\kappa = \frac{(\text{observed agreement} - \text{expected agreement})}{(100 - \text{expected agreement})} \tag{2.8}$$

Where:

$$\begin{aligned} \text{observed agreement} &= (nn + pp)/N \times 100 \\ \text{expected agreement} &= (Enn + Epp)/N \times 100 \end{aligned} \tag{2.9}$$

The values of κ were interpreted as a measure of agreement to a reference tract. κ is defined by Landis and Koch (1977) as follows: 0.11-0.2 as "slight", 0.21-0.4 as "fair", 0.41-0.60 as "moderate", 0.61-0.80 as "substantial", and 0.81-1.0 as "almost perfect" agreement.

2.4 Results and Discussion

The signature pattern of high radiality regions, observed at the white matter branches as they approach the cortex, was seen in all subjects. Figure 2.28 shows an enlarged section of the cortex where high radiality regions are seen at the apices of the gyri. This radiality metric was then used to guide a flood fill algorithm which filled regions which have higher radiality and are thus serve as optimal seed points for tractography. Figure 2.29 shows how an fMRI region is first confined to the grey matter, then dilated using RAFF.

The CST was utilised in testing for the initial evaluation of the Radiality Flood-Fill (RAFF). However, inconsistency in the motor cortex activity, as well as in the course of the CST through the brain made validation in the CST impracticable. This is due, in part, to the limitations of the deterministic fibre tracking method employed. There are regions along the CST, such as the passage through the Corona Radiata, where the fibres from the upper limb regions of the homunculus curve inferiorly and medially and intersect another tract; the Superior Longitudinal Fasciculus. In these regions, the principal eigenvector does not correspond to the true fibre directions (James *et al.*, 1999) and therefore the deterministic tractography method employed failed to show the true path of the finger tapping related

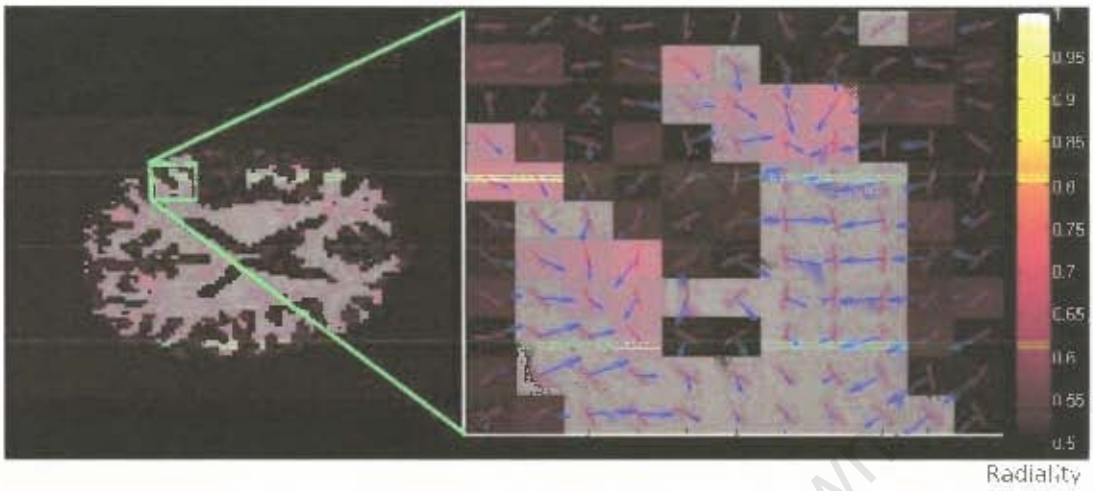

Figure 2.28: Radiality map overlaid on white matter probability slice showing principal diffusion direction (red lines) with the gradient vector across the white matter boundary (blue lines). High radiality (red voxels) is found where the PDD lines up with the gradient normal. A colour bar is shown with values ranging from zero to one (dimensionless).

fibres. The single tensor model can only reliably detect fibres going to the leg region and not those going to the upper extremity or facial regions (Qazi *et al.*, 2009). For this reason, Cohen's kappa was not applied to the CST tracts, since it was found that there was too much variation to obtain reliable tracts across individuals.

Since it was not viable to use the tracts from the finger tapping activations, solely the DMN was used to validate modified two-ROI with RAFF method. The DMN is the most robustly extracted of the resting state networks. In addition, the CB has been described previously as the major connection between the two main hubs of the DMN: the mPFC and the PCC (Greicius *et al.*, 2009; van den Heuvel *et al.*, 2009). From primate studies, this tract is known to be a direct connection which is not subject to crossing or branching. For these reasons it is a likely a more suitable tract for evaluating the validity of the modified two-ROI with RAFF method.

University of Cape Town

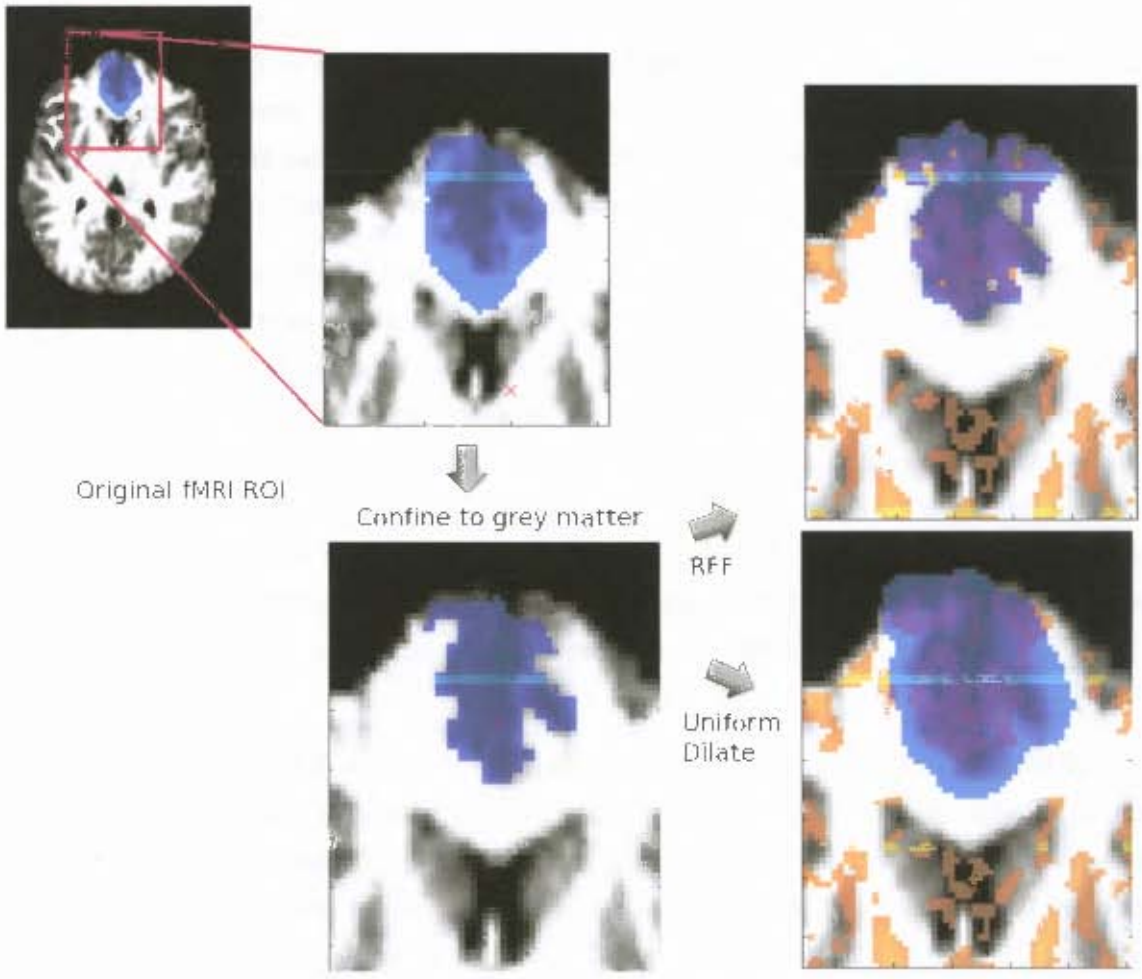

Figure 2.29: An example of radiality flood fill from an fMRI region. In this axial slice of a white matter probability image, the initial fMRI ROI (top left) is manipulated to grow into high radiality regions which are evident in orange. First the ROI is confined to the grey matter (using a WM probability threshold of <0.6) and then grown into high radiality regions using RAFF, based on a radiality threshold of >0.5. For comparison, a uniform dilation of three voxels is also shown.

Validation in the Default Mode Network

Table 2.1 shows results for a comparison between the landmark based two-ROI protocol of Wakana *et al.* (2007) and the modified two-ROI with RAFF approach. Table 2.2 presents a comparison between a two-ROI with uniform dilation and the landmark-based two-ROI protocol. This was done in order to compare the RAFF method to a comparable fMRI based approach. In both cases, all of the subjects showed "moderate" to "almost perfect" agreement according the Landis and Koch (1977) kappa scale. Figure 2.30 shows two examples where the tracts are seen to have substantial visual agreement.

The uniform dilation method extends the seed ROI into all the surrounding areas uniformly and produces more fibre tracts than RAFF. In spite of this, the increased number of fibres did not improve agreement with the landmark based two-ROI method when compared to the RAFF tool according to the kappa measure. As seen in table 2.2, consistently more fibres (n) were identified by the fMRI techniques. The number of computed fibres does not represent the true number of nerve fibres, so this increase in n does not reflect the accuracy of the tractography but rather the increased number of seed points used in the fMRI techniques. The kappa measure reflects high levels of agreement and, based on a one-sample t-test, shows no significant difference as compared to the uniform dilation method.

University of Cape Town

The two-ROI with RAFF method has several advantages over the landmark based two-ROI protocol. The first ROI is defined by the fMRI activation so there was no subjective input from the user at this stage. With the resulting tracts displayed on the screen, it is then possible to "trim" the desired tracts using the logical AND with ROI 2 (as described in Section 2.26). The AND operation provides a strong degree of specificity of the resulting tracts and this step is made less subjective since only the general anatomical course of the tract needs to be known. While the two-ROI with uniform dilation shares these advantages, it is a less specific means to define the seed ROI than with RAFF.

While the kappa measures show high levels of agreement, the number of fibres produced using both RAFF and uniform dilation of fMRI seeds resulted in noticeably higher numbers of fibres (n) than the landmark based two-ROI method. Achieving high values of kappa accounts for this since many of these fibres overlap.

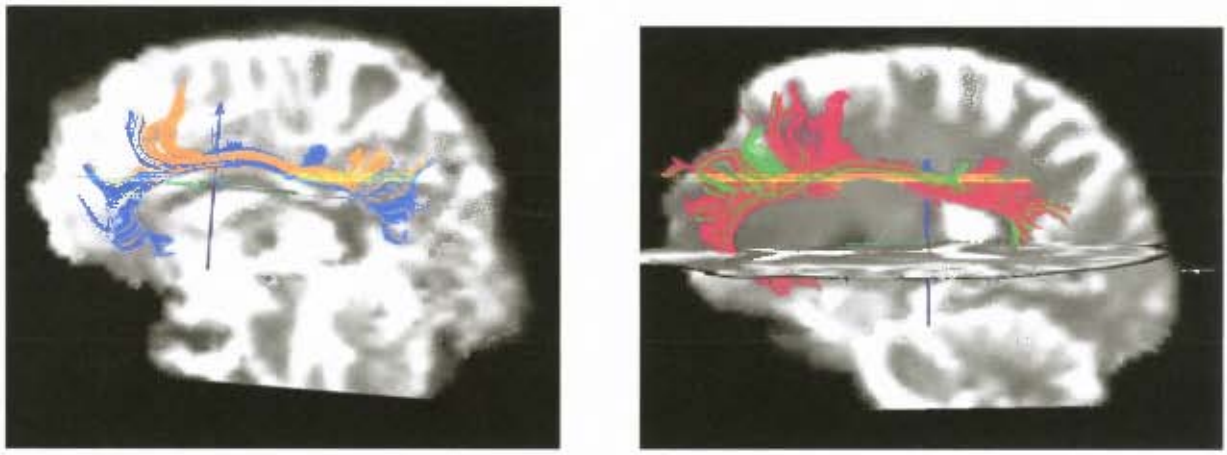

(a) (b)

Figure 2.30: (a) Visual evidence of agreement between methods for subject 2 confirm "substantial" agreement measures for κ. The yellow fibres were extracted using the RAFF method and the blue fibre using the landmark based two-ROI method. In (b), κ values for subject 3 indicate "almost perfect" agreement. Red fibres were extracted using the RAFF method and the green fibres using the landmark based two-ROI method.

	κ left CB	κ right CB	Left RAFF (n)	Right RAFF (n)	Left-Landmark (n)	Right-Landmark (n)
subject 1	0.5941	0.5758	103	56	38	46
subject 2	0.6812	0.8090	122	114	50	79
subject 3	0.8002	0.8494	185	117	76	63
subject 4	0.7462	0.6194	257	124	85	45
subject 5	0.6973	0.8198	201	67	42	44
subject 6	0.6974	0.6758	287	97	78	34
subject 7	0.8207	0.4861	202	13	27	3
subject 8	0.6319	0.7119	78	9	63	14
subject 9	0.6734	0.5479	127	35	71	48
subject 10	0.6549	0.6640	46	38	98	56
subject 11	0.5675	0.7348	139	382	70	92
Mean κ	0.6877	0.6813				

Table 2.1: Kappa measure of agreement between tracts derived from two-ROI with RAFF and tracts derived from the landmark based two-ROI method (n is the total number of fibres in the resulting tracts).

	κ left CB	κ right CB	Left unif. dilate (n)	Right unif. dilate (n)	Left Landmark (n)	Right Landmark (n)
subject 1	0.5818	0.4678	74	124	38	46
subject 2	0.5066	0.7668	179	170	50	79
subject 3	0.7671	0.8313	403	360	76	63
subject 4	0.6963	0.6315	400	330	85	45
subject 5	0.6449	0.8655	358	75	42	44
subject 6	0.7936	0.5761	155	27	78	34
subject 7	0.6707	0.358	368	27	27	3
subject 8	0.7594	0.7599	214	19	63	14
subject 9	0.7747	0.4608	55	6	71	48
subject 10	0.675	0.684	214	130	98	56
subject 11	0.6582	0.7167	590	596	70	92
Mean κ	0,6844	0,6471				

Table 2.2: Kappa measure of agreement between tracts derived from two-ROI with a uniform dilation and tracts derived from the landmark based two-ROI method (n is the total number of fibres in the resulting tracts).

Chapter 3

Case Study: Application to Default Mode Network Connectivity in Urbach-Wiethe Disease

University of Cape Town

3.1 Introduction

The goal of this case study was to show that the modified two-ROI method with RAFF would be successful in analysing the structural connectivity underlying fMRI activity in a clinical cohort. Although Chapter 2 showed that the RAFF method produced tracts of significant similarity to purely anatomically derived tracts, when looking for group differences, the risk of subjectivity with manually placed seeds is a confounding factor. Using the validated RAFF protocol for extracting the CB from DMN activity, tract integrity measured by mean FA may be obtained in a more objective way.

Urbach Wiethe Disease (UWD), also called Lipoid Proteinosis, is an autosomal recessive disorder that causes gradual bilateral calcification of the amygdala. In UWD, there is a bilateral lesion of a highly interconnected part of the brain, the amygdala. In the UWD sample used in this study (described in more detail below) there are no gross behavioural, emotional, intellectual or social impairments. For this reason, WM connections not directly linked to the

amygdala may be unaffected by the lesion. To test this hypothesis, the CB connecting the two most prominent nodes of the Default Mode Network (mPFC and PCC) was chosen as a candidate WM tract for comparison with normal controls. The CB was readily extracted from fMRI data and DTI tractography using the techniques developed in Chapter 2. Mean FA of the CB, as a marker of WM integrity, was measured in UWD compared to normal controls.

3.2 Background

Based on the comparison of DTI metrics, such as FA, inferences can be made about the integrity of WM tracts. In direct WM pathologies, variations in FA could be due to demyelination, axonal damage, microstructural reorganisation, dislocation, swelling, inflammation or disruption of the axonal fibres. In addition to the application of DTI to direct pathology, disruptions in connectivity have been observed in the WM in primary psychiatric disorders (Filley, 2005). It was Carl Wernicke who was first to recognise that psychiatric disorders were a consequence of disruption in the long-range WM connections, he called these disruptions of connectivity "sejunctions" (Frith, 2004). More recently, using modern imaging tools such as DTI, schizophrenia, dyslexia and autism have all been described as disconnection syndromes (Courchesne and Pierce, 2005), in that certain WM tracts integral to normal brain function have shown marked microstructural differences. FA data have even been correlated with measures of overall intelligence (Yu *et al.*, 2008).

University of Cape Town

Urbach-Wiethe Disease and the Amygdala

UWD is of special interest to neuroscience as it is the only human model of a discrete, selective, bilateral, stable, non-neurodegenerative stereotyped lesion anywhere in the brain. This disease presents in early infancy with a hoarse voice owing to thickening of the vocal cords and subsequently, in early childhood, with characteristic pox like markings and thickening of the skin.

Severe emotional behaviour deficits in a single UWD case known in the literature as "SM" (Adolphs *et al.*, 1995, 2005; Kennedy *et al.*, 2009; Todd and Anderson, 2009; Feinstein *et al.*, 2010), have made the amygdala the focus of intense interest in the field of affective neuroscience. The findings in SM regarding fear response conditioning (Feinstein *et al.*, 2010) have been supported by bilateral amygdalectomy studies in rhesus monkeys (Emery *et al.*, 2001). Based largely on this single human case and the primate studies, the amygdala is considered to be a critical centre of the emotional and social brain (Phelps, 2004; Todd and Anderson, 2009). This research has shown that the amygdala is widely and intricately connected as a hub of connectivity (Ashwin *et al.*, 2007).

The vast majority of UWD cases amenable to scientific investigation (approximately 50) reside in the Northern Cape Province of South Africa. Recent investigations in a group of five South African UWD patients with no secondary psychopathology is adding important new details to the understanding of the human amygdala. As shown in Figure 3.1, structural MRI results in these subjects shows calcification limited to the Basolateral Amygdala (BLA). Functional MRI shows activity in the Superficial Amygdala (SFA) and Centromedial Amygdala (CMA) sub-regions, but not in the BLA, in response to emotional face stimuli (Terburg *et al.*, 2011). In contrast to the single case mentioned above, behavioural studies of emotional stimuli processing reveal no gross deficits in emotional or social function in these patients. Nevertheless, volume loss in PFC regions that normally share reciprocal connections with the amygdala has been observed (B. Morgan, pers. comm, January 2011). These amygdala and PFC changes with little evidence of loss of function make these UWD subjects ideal candidates for validating neuroimaging tools.

University of Cape Town

Hypothesis: Global or Local Connectivity Changes

Importantly, in UWD, the surrounding brain structures remain preserved. It must be assumed, however, that the primary connections of the amygdala are affected (its afferent and efferent projections). The amygdala is one of the most extensively interconnected regions of the brain and if amygdala tissue is lost due to a lesion then a question is whether or not

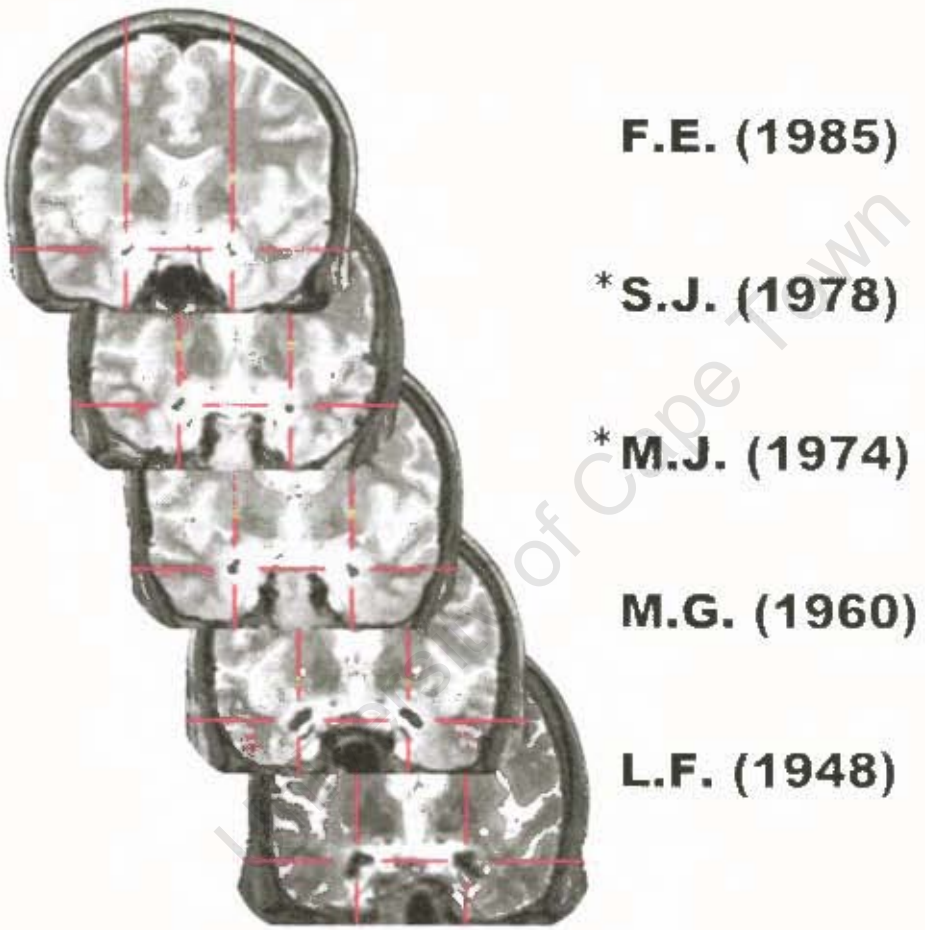

University of Cape Town

Figure 3.1: T2 weighted structural (coronal view) of five UWD subjects with birth year and cross-hairs indicating the progression of the calcified amygdala regions with age. Two of the subjects (marked with *) were part of the fMRI/DTI cohort in this thesis. Image courtesy of Terburg *et al.* (2011).

the other core networks of the brain are affected. The DMN serves as an ideal network to measure global connectivity differences, since it has been proposed that it is the structural core network which underlies the human cerebral cortex (Hagmann *et al.*, 2008).

The investigation aims to discover possible alterations of the DMN in response to the loss of an important component of the brain. The following question was addressed: is there secondary loss of WM connectivity in a pathway (CB) connecting two structures (PCC and mPFC), where one of them (mPFC) is normally strongly and reciprocally connected to the amygdala?

3.3 Methods

The study cohort was comprised of five UWD subjects and nine controls. Subjects had no physical illness or psychopathology and were matched for age, sex, education and IQ. Subject age and level of education is shown in Table 3.1. Ethics approval was originally obtained from the University of Stellenbosch ethics committee (reference number 2002/C103), as part of a larger parent study of UWD. Written informed consent was obtained from all subjects. Since more females than males were available, only females were used in order to limit the complexity of the data. The fMRI and DTI data were acquired in the manner described in Chapter 2.

University of Cape Town

The CB's of all subjects were extracted using the two-ROI with RAFF method as described in Section 2.3.4. Mean FA along the length of the tract was compared between the groups. FA was the only DTI metric chosen to measure structural connectivity, since it has been suggested that FA is the most specific DTI metric related to tract integrity underlying network connectivity (Teipel *et al.*, 2010).

Global, data driven methods were applied to the data in order to validate the CB connectivity findings. First, as described in Appendix A, the resting state fMRI data were used in a group ICA analysis using the GIFT package (Calhoun *et al.*, 2001). Tract Based Spatial Statistics (TBSS) methods were applied to the FA data, which allows global comparison of white matter microstructure between groups while accounting for confounding intersubject

Patients	Age	Schooling years
patient 1	32	9
patient 2	35	12
patient 3	29	10
patient 4	60	8
patient 5	40	7
Controls		
Control 1	34	12
Control 2	29	9
Control 3	43	11
Control 4	23	12
Control 5	29	9
Control 6	43	9
Control 7	35	12
Control 8	38	7
Control 9	21	12

Table 3.1: The patients and controls were matched for age, sex and education (except for patient 4 who is 60 years old). In this table, ages and number of years in school are shown for the control and UWD subject cohort.

coregistration steps (Smith *et al.*, 2006). The TBSS procedure and results are detailed in Appendix B. Since these methods could be readily applied using the available data and were performed using standard parameter settings, they provided a non-biased way to validate connectivity findings in the CB.

3.4 Results and Discussion

The resulting DMN activity maps from group ICA (as described in Appendix A) are shown in Figure 3.2 and Figure 3.3. Figure 3.2 shows that the group DMN activity pattern in UWD subjects is largely consistent with that of the control group, shown in Figure 3.3. The preliminary investigation of the DMN fMRI data between the control and UWD groups (Appendix A) shows increased activity in the right PCC in UWD, which warrants further investigation. However these differences were not apparent after correcting for multiple comparisons.

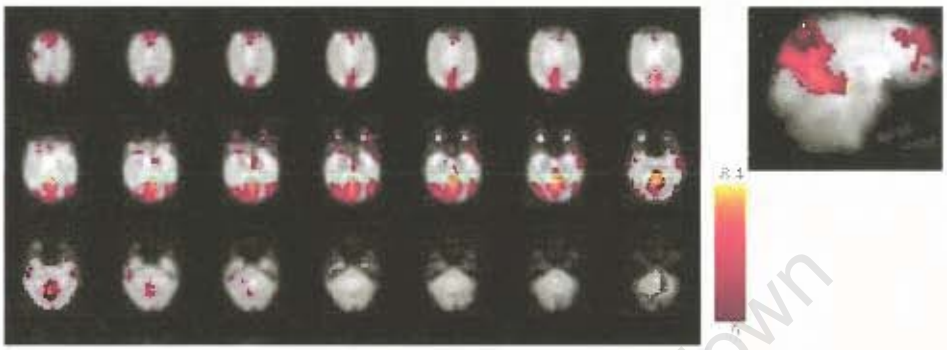

Figure 3.2: The DMN activation for UWD subjects shows activation of the DMN consistent with the normal control group in Figure 3.3.

University of Cape Town

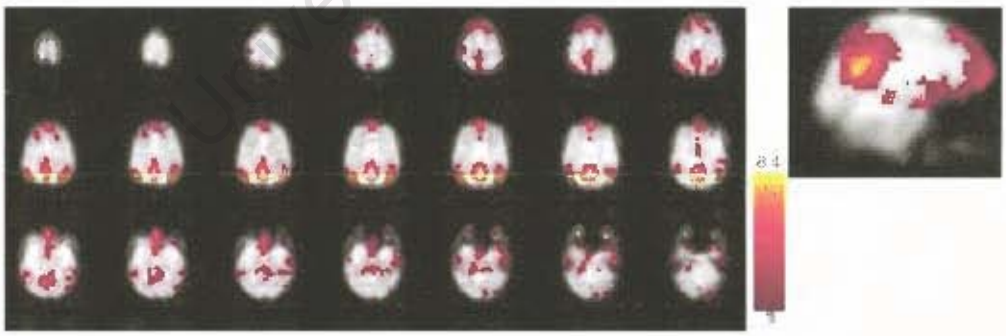

Figure 3.3: The group DMN activation for normal control subjects shows DMN activity on axial slices and with an enlarged sagittal view. The colour bar shows the Z-statistic intensity.

Using the CBs extracted from all subjects, as shown in Figure 3.4, the mean FA was measured for UWD subjects and controls. Table 3.2 presents these results. No statistically significant differences between groups on overall (left and right combined) or unilateral CBs were found. The results in Table 3.2 is represented as a bar plot in Figures 3.5, 3.6 and 3.7. It may be noted, however, that the mean FA along the right side of the CB in Figure 3.6 only just fails to reach a significance of $p < 0.05$.

Global white matter integrity, as measured by TBSS (Appendix B), also showed no significant white matter group differences after correcting for multiple comparisons (using Threshold Free Cluster Enhancement (TFCE), $p < 0.05$). The uncorrected results ($p < 0.05$) show reduced FA in the right anterior region of the CB.

Three independent methods thus found indications that the structure and/or function of the DMN may be different in UWD versus controls: mean FA in the CB tract fibres, FA differences in the CB using TBSS, and group resting state fMRI. All three methods show these differences to be more evident in the right hemisphere than in the left hemisphere.

Compared with the behavioural deficits seen in UWD subject SM, the evidence of normal WM connectivity in this group supports the normal behavioural observations. Viewing the CB as a proxy for global brain connectivity, the results suggest normal DMN connectivity and therefore intact global connectivity. Since SM has a complete lesion of all amygdala nuclei and her brain damage is not limited to the amygdala, her abnormal behavioural measures could be due to a combination of the amygdala lesion, and damage to adjacent structures such as the entorhinal cortex and connecting white matter (Feinstein *et al.*, 2010). The results of normal white matter connectivity from this study, in contrast, were applied to a group of UWD subjects and support recent findings that there is residual functional activity in the amygdala (Terburg *et al.*, 2011). However, since no fMRI or DTI data have been acquired for SM, it is not possible to comment further.

University of Cape Town

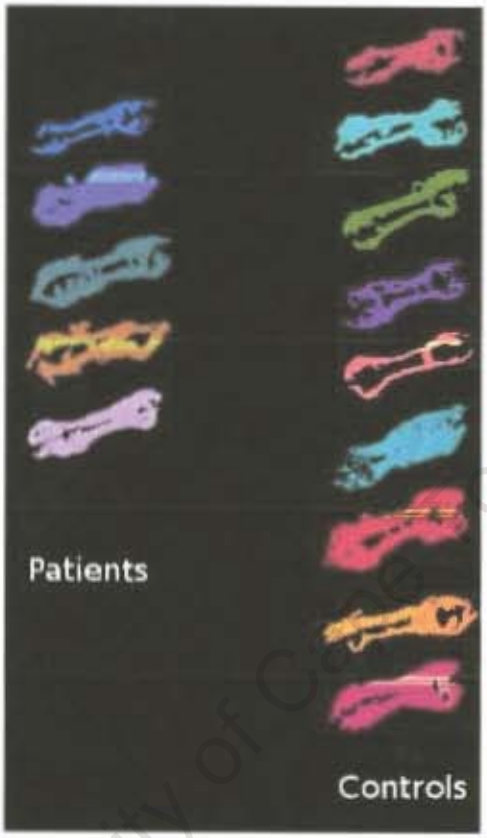

Figure 3.4: Cingulum bundles of all subjects.

University of Cape Town

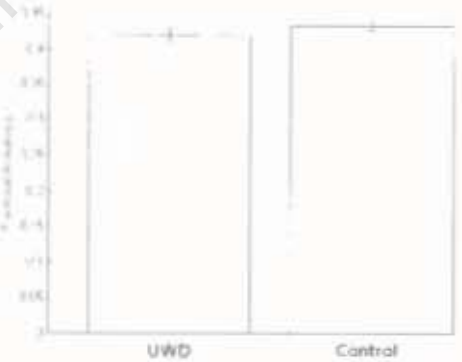

Figure 3.5: Mean fractional anisotropy within both sides of the Cingulum Bundle. Includes five UWD subjects and nine control subjects. p = 0.2042 (The p-value is the probability, under the null hypothesis, of observing a value as extreme or more extreme of the two-sample t-test statistic).

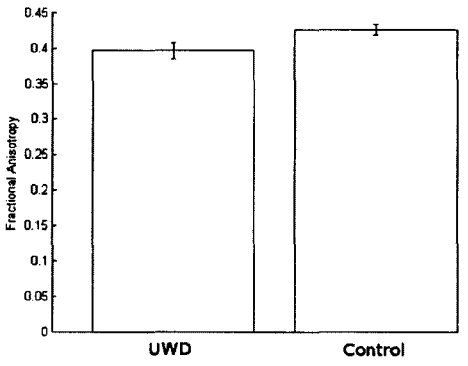

Figure 3.6: Mean FA within the right Cingulum Bundle. Includes five UWD subjects and nine control subjects. p = 0.0569

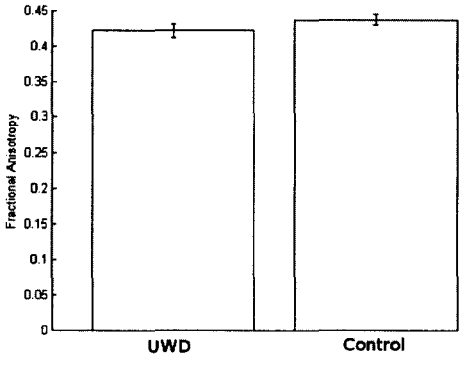

Figure 3.7: Mean FA within the left Cingulum Bundle. Includes five UWD subjects and eight control subjects. p = 0.2347.

	Control	UWD
Left and right combined	0.433 ± 0.006	0.418 ± 0.009
Left	0.436 ± 0.007	0.421 ± 0.010
Right	0.425 ± 0.008	0.396 ± 0.012

Table 3.2: Mean FA over both left and right CB's.

Chapter 4

Conclusion and Outlook

University of Cape Town

Though validation is complicated by the absence of a ground truth model for DTI tractography, the modified two-ROI with RAFF approach can still be evaluated in terms of its functionality, usability and reproducibility in relation to current practice. Using Cohen's kappa, the tracts resulting from the approach presented in this thesis were found to have high spatial agreement with the landmark based two-ROI protocol of Wakana *et al.* (2007), which represents current practice. The two-ROI with RAFF approach is semi-automated, requiring no subjective manipulation of starting ROIs since they are defined first by fMRI and then automatically grown into the WM. The mrDiffusion platform with the RAFF enhancements for incorporating fMRI activity maps is easy to use within the fMRI/DTI data processing pipeline.

Once validated as being sufficiently similar to current practice, the two-ROI with RAFF approach was applied to a study of Urbach-Wiethe Disease. In order to evaluate the effects of the disease on brain connectivity, the CB was evaluated from DMN fMRI activations since it represents the degree to which the global DMN activity has been affected by bilateral basolateral amygdala calcification. No significant differences were found between UWD subjects and matched controls, however WM differences in the right CB just fell short of reaching significance. There were also no significant differences noted using data driven analyses in TBSS and group ICA of resting state fMRI, confirming the CB fibre tracking result. Intact connectivity in this intrinsic brain network supports the lack of gross behavioural deficits

observed in this cohort of UWD subjects.

It is worth noting that three independent methods (mean FA in the CB tract fibres, FA differences in the CB using TBSS, and group resting state fMRI) indicated that there may be some differences between UWD and matched controls in the statistics in the right hemisphere. Although these results do not reach levels of statistical significance, there are trends which agree across the three methods. This warrants further investigation in a larger cohort.

If a difference is confirmed in future studies of UWD, this would indicate the there may be functional compensation in response to structural alteration in secondary circuits (i.e. circuits not directly involving the amygdala). The fact that this cohort is grossly behaviourally normal does not necessarily imply that there have been no structural and/or functional changes in secondary circuits. The preservation of normal behaviour could be due to structural and/or functional neuroplastic compensatory changes that are too subtle to be unambiguously detected by the two-ROI with RAFF method. Nevertheless, if future investigations confirm the above-mentioned right hemisphere trends the validity of two-ROI with RAFF will be further established.

Future studies investigating DTI at the GM/WM interface may make use of higher resolutions of DTI, enabling the viewing of finer details of the fibre systems, particularly at the fibre origins and terminations where the radial structure of the minicolumns and axons intersperse with tangential dendrites and interneurons. Alternative methods of tracing fibres such as HARDI and a multiple tensor model (Tuch *et al.*, 2003a) would also further our understanding since multiple coherent fibre populations are discernible in each voxel. Further insight may be gained by using DTI with varying ranges of acquisition parameters which have been shown to discern different cellular details, such as in low anisotropy regions (Rane *et al.*, 2010).

Refinement of the flood-fill segmentation method with more sophisticated algorithms such as level sets or statistical surface evolution (Lenglet *et al.*, 2006) will be required to realise the full potential for combining fMRI and DTI at the current spatial resolutions. However,

University of Cape Town

the use of radiality with flood-fill to seed DTI tractography from fMRI, as presented in this thesis serves as an encouraging proof of concept which will hopefully kindle further research in this field.

References

Adolphs, R., Gosselin, F., Buchanan, T., Tranel, D., Schyns, P., Damasio, A., 2005. A mechanism for impaired fear recognition after amygdala damage. *Nature* 433 (7021), 68–72.

Adolphs, R., Tranel, D., Damasio, H., Damasio, A., 1995. Fear and the human amygdala. *Journal of Neuroscience* 15 (9), 5879.

Andersson, J., Skare, S., Ashburner, J., 2003. How to correct susceptibility distortions in spin-echo echo-planar images: application to diffusion tensor imaging. *Neuroimage* 20 (2), 870–888.

Andersson, J., Smith, S., Jenkinson, M., 2007a. Non-linear optimisation. *FMRIB technical report TR07JA1* .
URL `www.fmrib.ox.ac.uk/analysis/techrep`

Andersson, J., Smith, S., Jenkinson, M., 2007b. Non-linear registration, aka Spatial normalisation. *FMRIB technical report TR07JA2* .
URL `www.fmrib.ox.ac.uk/analysis/techrep`

Anwander, A., Pampel, A., Knösche, T., 2009. High Resolution Diffusion-Weighted Imaging Reveals Variable Cortex Anisotropy in Humans. *NeuroImage* 47 (Supplement 1), S51.

Arnone, D., Barrick, T., Chengappa, S., Mackay, C., Clark, C., Abou-Saleh, M., 2008. Corpus callosum damage in heavy marijuana use: preliminary evidence from diffusion tensor tractography and tract-based spatial statistics. *Neuroimage* 41 (3), 1067–1074.

Ashwin, C., Baron-cohen, S., Wheelwright, S., Riordan, M. O., Bullmore, E. T., 2007. Differential activation of the amygdala and the social brain during fearful face-processing in Asperger Syndrome. *Neuropsychologia* 45, 2–14.

University of Cape Town

Assaf, M., Jagannathan, K., Calhoun, V., Miller, L., Stevens, M., Sahl, R., O'Boyle, J., Schultz, R., Pearlson, G., 2010. Abnormal functional connectivity of default mode subnetworks in autism spectrum disorder patients. *NeuroImage* 53, 247–256.

Assaf, Y., Pasternak, O., 2008. Diffusion tensor imaging (DTI)-based white matter mapping in brain research: a review. *Journal of Molecular Neuroscience* 34 (1), 51–61.

Basser, P., Pajevic, S., Pierpaoli, C., Duda, J., Aldroubi, A., 2000. In vivo fibre tractography using DT-MRI data. *Magnetic Resonance in Medicine* 44 (4), 625–632.

Beaulieu, C., 2002. The basis of anisotropic water diffusion in the nervous system–a technical review. *NMR in Biomedicine* 15 (7-8), 435–455.

Behrens, T., Woolrich, M.W Jenkinson, M., Johansen-Berg, H., Nunes, R., Clare, S., Matthews, P., Brady, J., Smith, S., 2003. Characterization and propagation of uncertainty in diffusion-weighted mr imaging. *Magnetic Resonance in Medicine* 50, 1077–1088.

Bell, A., Sejnowski, T., 1995. An information-maximization approach to blind separation and blind deconvolution. *Neural Computation* 7 (6), 1129–1159.

Broyd, S., Demanuele, C., Debener, S., Helps, S., James, C., Sonuga-Barke, E., 2009. Default-mode brain dysfunction in mental disorders: a systematic review. *Neuroscience & Biobehavioral Reviews* 33 (3), 279–296.

Buckner, R. L., Andrews-Hanna, J. R., Schacter, D. L., 2008. The default network: Anatomy, function, and relevance to disease. *Annals of the New York Academy of Sciences* 1124 (1), 1–38.

Buxhoeveden, D. P., Casanova, M. F., 2002. The minicolumn hypothesis in neuroscience. *Brain* 125, 935–951.

Calhoun, V., Adali, T., Pearlson, G., Pekar, J., 2001. A method for making group inferences from functional MRI data using independent component analysis. *Human Brain Mapping* 14 (3), 140–151.

Clark, C., Barrick, T., Murphy, M., Bell, B., 2003. White matter fibre tracking in patients with space-occupying lesions of the brain: a new technique for neurosurgical planning? *Neuroimage* 20 (3), 1601–1608.

University of Cape Town

Cohen, A., Fair, D., Dosenbach, N., Miezin, F., Dierker, D., Van Essen, D., Schlaggar, B., Petersen, S., 2008. Defining functional areas in individual human brains using resting functional connectivity MRI. *Neuroimage* 41 (1), 45–57.

Courchesne, E., Pierce, K., 2005. Why the frontal cortex in autism might be talking only to itself: local over-connectivity but long-distance disconnection. *Current Opinion in Neurobiology* 15 (2), 225–230.

Dauguet, J., Peled, S., Berezovskii, V., Delzescaux, T., Warfield, S., Born, R., Westin, C., 2006. 3D Histological Reconstruction of fibre Tracts and Direct Comparison with Diffusion Tensor MRI Tractography. *Lecture Notes in Computer Science* 4190, 109.

DeFelipe, J., Rockland, K. S., Fields, R. D., Hof, P. R., Höistad, M., Kostovic, I., Meyer, G., Rockland, K. S., 2010. Cortical white matter : beyond the pale remarks , main conclusions and discussion. *Frontiers in Neuroanatomy* 4 (4), 1–28.

Duffau, H., Capelle, L., Denvil, D., Sichez, N., Gatignol, P., Taillandier, L., Lopes, M., Mitchell, M., Roche, S., Muller, J., *et al.*, 2003. Usefulness of intraoperative electrical subcortical mapping during surgery for low-grade gliomas located within eloquent brain regions: functional results in a consecutive series of 103 patients. *Journal of Neurosurgery* 98 (4), 764–778.

Emery, N., Capitanio, J., Mason, W., Machado, C., Mendoza, S., Amaral, D., 2001. The effects of bilateral lesions of the amygdala on dyadic social interactions in rhesus monkeys (Macaca mulatta). *Behavioral Neuroscience* 115 (3), 515.

Feinstein, J., Adolphs, R., Damasio, A., Tranel, D., 2010. The human amygdala and the induction and experience of fear. *Current Biology* 21, 34–38.

Filley, C. M., 2005. Neurobehavioral Aspects of Cerebral White Matter Disorders. *Psychiatric Clinics of North America* 28, 685–700.

Fox, M. D., Raichle, M. E., 2007. Spontaneous fluctuations in brain activity observed with functional magnetic resonance imaging. *Nature Reviews, Neuroscience* 8 (9), 700–711.

Fransson, P., Marrelec, G., 2008. The precuneus/posterior cingulate cortex plays a pivotal role in the default mode network: Evidence from a partial correlation network analysis. *NeuroImage,* 42 (3), 1178–1184.

University of Cape Town

Friston, K., Frith, C., Liddle, P., Frackowiak, R., 1993a. Functional connectivity: the principal component analysis of large (pet) data sets. *Journal of Cerebral Blood Flow and Metabolism* 13, 5–14.

Frith, C., 2004. Is autism a disconnection disorder? *The Lancet* 3, 577.

Ghashghaei, H. T., Lai, C., Anton, E. S., 2007. Neuronal migration in the adult brain: are we there yet? *Nature Neuroscience* 8 (2), 141–151.

Greicius, M., 2008. Resting-state functional connectivity in neuropsychiatric disorders. *Current Opinion in Neurology* 21, 424–430.

Greicius, M., Krasnow, B., Reiss, A., Menon, V., 2003. Functional connectivity in the resting brain: a network analysis of the default mode hypothesis. *Proceedings of the National Academy of Sciences* 100 (1), 253–258.

Greicius, M., Supekar, K., Menon, V., Dougherty, R., 2009. Resting-state functional connectivity reflects structural connectivity in the default mode network. *Cerebral Cortex* 19 (1), 72–78.

Hagmann, P., Cammoun, L., Gigandet, X., Meuli, R., Honey, C., Wedeen, V., Sporns, O., 2008. Mapping the Structural Core of Human Cerebral Cortex. *PLoS Biology* 6 (7), e159.

Hagmann, P., Jonasson, L., Maeder, P., Thiran, J., Wedeen, V., Meuli, R., 2006. Understanding diffusion mr imaging techniques: From scalar diffusion-weighted imaging to diffusion tensor imaging and beyond. *Radiographics* 26, S205–S223.

Hattingen, E., Rathert, J., Jurcoane, A., Weidauer, S., Szelényi, A., Ogrezeanu, G., Seifert, V., Zanella, F., Gasser, T., 2009. A standardised evaluation of pre-surgical imaging of the corticospinal tract: where to place the seed ROI. *Neurosurgical Review* 32 (4), 445–456.

Horwitz, B., 2003. The elusive concept of brain connectivity. *NeuroImage* 19, 466 – 470.

Jaermann, T., De Zanche, N., Staempfli, P., Pruessmann, K. P., Valavanis, A., Boesiger, P., Kollias, S. S., 2008. Preliminary Experience with Visualization of Intracortical fibres by Focused High-Resolution. *American Journal Of Neuroradiology* 29, 146–150.

University of Cape Town

James, D. A., Alex, D., Gee, J., Bajcsy, R., 1999. Similarity measures for matching diffusion tensor images. In: *Proceedings of the British Machine Vision Conference (BMVC)*, pp. 93–102, pp. 93–102.

Jellison, B. J., Field, A. S., Medow, J., Lazar, M., Salamat, M. S., Alexander, A. L., 2004. Diffusion Tensor Imaging of Cerebral White Matter: A Pictorial Review of Physics, fibre Tract Anatomy, and Tumor Imaging Patterns. *American Journal of Neuroradiology* 25 (3), 356–369.

Johansen-Berg, H., 2001. *Reorganisation and modulation of the human sensorimotor system: implications for recovery of motor function after stroke*. Ph.D. thesis, University of Oxford.

Johnston, J. M., Vaishnavi, S. N., Smyth, M. D., Zhang, D., He, B. J., Zempel, J. M., Shimony, J. S., Snyder, A. Z., Raichle, M. E., 2008. Loss of resting interhemispheric functional connectivity after complete section of the corpus callosum. *Journal of Neuroscience* 28 (25), 6453–6458.

Joseph, R., Heckers, S., 1996. *Neuropsychiatry, neuropsychology, and clinical neuroscience: Emotion, evolution, cognition, language, memory, brain damage, and abnormal behavior*. Williams & Wilkins.

Kamada, K., Todo, T., Masutani, Y., Aoki, S., Ino, K., Takano, T., Kirino, T., Kawahara, N., Morita, A., 2005. Combined use of tractography-integrated functional neuronavigation and direct fibre stimulation. *Journal of Neurosurgery* 102 (4), 664–672.

Kennedy, D., Gläscher, J., Tyszka, J., Adolphs, R., 2009. Personal space regulation by the human amygdala. *Nature Neuroscience* 12 (10), 1226–1227.

Kim, D., Kim, M., 2005. Combining functional and diffusion tensor mri. *Annals of the New York Academy of Sciences* 1064, 1–15.

Kim, J. H., Loy, D. N., Liang, H.-F., Trinkaus, K., Schmidt, R. E., Song, S.-K., 2007. Noninvasive diffusion tensor imaging of evolving white matter pathology in a mouse model of acute spinal cord injury. *Magnetic Resonance in Medicine* 58 (2), 253–260.

Kollias, S. S., Alkadhi, H., Jaermann, T., Crelier, G., Hepp-Reymond, M.-C., 2001. Identification of multiple nonprimary motor cortical areas with simple movements. *Brain Research Reviews* 36 (2-3), 185–195.

University of Cape Town

Landis, J. R., Koch, G. G., 1977. The Measurement of Observer Agreement for Categorical Data Data for Categorical of Observer Agreement The Measurement. *Biometrics* 33 (1), 159–174.

Leclercq, D., Duffau, H., Capelle, L., Delmaire, C., Gatignol, P., Ducros, M., Lehericy, S., 2010. Comparison of diffusion tensor imaging tractography of language tracts with intraoperative subcortical stimulations. *Journal of Neurosurgery* 112, 503–511.

Lenglet, C., Member, S., Rousson, M., Deriche, R., 2006. DTI Segmentation by Statistical Surface Evolution. *IEEE Transactions On Medical Imaging* 25 (6), 685–700.

Li, Y., Adali, T., Calhoun, V., 2007. A feature-selective independent component analysis method for functional MRI. *Journal of Biomedical Imaging* (2), 1–12.

Logothetis, N., Wandell, B., 2004. Interpreting the BOLD Signal. *Annual Review of Physiology* 66, 735–769.

McKinstry, R. C., Mathur, A., Miller, J. H., Ozcan, A., Snyder, A. Z., Schefft, G. L., Almli, C. R., Shiran, S. I., Conturo, T. E., Neil, J. J., 2002. Radial Organization of Developing Preterm Human Cerebral Cortex Revealed by Non-invasive Water Diffusion Anisotropy MRI. *Cerebral Cortex* 12, 1237–1243.

Mcnab, J. A., Jbabdi, S., Deoni, S. C. L., Douaud, G., Behrens, T. E. J., Miller, K. L., 2009. NeuroImage High resolution diffusion-weighted imaging in fixed human brain using diffusion- weighted steady state free precession. *NeuroImage* 46, 775–785.

Mori, S., Crain, B., Chacko, V., Van Zijl, P., 1999. Three-dimensional tracking of axonal projections in the brain by magnetic resonance imaging. *Annals of Neurology* 45 (2), 265–269.

Mori, S., van Zijl, P., 2002. Fiber tracking: principles and strategies–a technical review. *NMR in Biomedicine* 15 (7-8), 468–480.

Mori, S., Zhang, J., 2006. Principles of Diffusion Tensor Imaging and Its Applications to Basic Neuroscience Research. *Neuron* 51 (5), 527–539.

Mukherjee, P., Miller, J., Shimony, J., Conturo, T., Lee, B., Almli, C., McKinstry, R., 2001. Normal Brain Maturation during Childhood: Developmental Trends Characterized with Diffusion-Tensor MR Imaging1. *Radiology* 221 (2), 349.

University of Cape Town

Mulkern, R. V., Davis, P. E., Haker, S. J., San, R., Estepar, J., Panych, L. P., Maier, S. E., Rivkin, M. J., 2006. Complementary aspects of diffusion imaging and fMRI: structure and function. *Magnetic Resonance Imaging* 24, 463 – 474.

Noback, C., 2005. *The human nervous system: structure and function*. Humana Press Inc.

Ozturk, A., Sasson, A., Farrell, J., Landman, B., da Motta, A., Aralasmak, A., Yousem, D., 2008. Regional differences in diffusion tensor imaging measurements: assessment of intrarater and interrater variability. *American Journal of Neuroradiology* 29 (6), 1124–1127.

Parker, G., Stephan, K., Barker, G., Rowe, J., MacManus, D., Wheeler-Kingshott, C., Ciccarelli, O., Passingham, R., Spinks, R., Lemon, R., *et al.*, 2002. Initial demonstration of in vivo tracing of axonal projections in the macaque brain and comparison with the human brain using diffusion tensor imaging and fast marching tractography. *Neuroimage* 15 (4), 797–809.

Penfield, C., 1950. The Cerebral Cortex of Man: A Clinical Study of Localization of Function. *Journal of the American Medical Association* 144 (16), 1412.

Phelps, E. A., 2004. Human emotion and memory : interactions of the amygdala and hippocampal complex. *Current Opinion in Neurobiology* 14, 198–202.

Qazi, A., Radmanesh, A., O'Donnell, L., Kindlmann, G., Peled, S., Whalen, S., Westin, C., Golby, A., 2009. Resolving crossings in the corticospinal tract by two-tensor streamline tractography: Method and clinical assessment using fMRI. *NeuroImage* 47, T98–T106.

Rakic, P., 2003. Elusive Radial Glial Cells : Historical and Evolutionary Perspective. *Glia* 43, 19 –32.

Rakic, P., 2007. The radial edifice of cortical architecture : From neuronal silhouettes to genetic engineering. *Brain Research Reviews* 55, 204–219.

Ramnani, N., Behrens, T., Penny, W., Matthews, P., 2004. New approaches for exploring anatomical and functional connectivity in the human brain. *Society of Biological Psychiatry* 56, 613–619.

Rane, S., Nair, G., Duong, T. Q., 2010. DTI at long diffusion time improves fibre tracking. *NMR in Biomedicine* 23 (5), 459–465.

University of Cape Town

Ronen, I., Kim, K., Garwood, M., Ugurbil, K., Kim, D., 2003. Conventional DTI vs. slow and fast diffusion tensors in cat visual cortex. *Magnetic Resonance in Medicine* 49 (5), 785–790.

Rueckert, D., Sonoda, L. I., Hayes, C., Hill, D. L. G., Leach, M. O., Hawkes., D. J., 1999. Non-rigid registration using free-form deformations: Application to breast MR images. *IEEE Transactions on Medical Imaging* 18 (8), 712–721.

Rykhlevskaia, E., Gratton, G., Fabiani, M., 2008. Combining structural and functional neuroimaging data for studying brain connectivity: A review. *Psychophysiology* 45 (2), 173–187.

Smith, S., Jenkinson, M., Johansen-Berg, H., Rueckert, D., Nichols, T., Mackay, C., Watkins, K., Ciccarelli, O., Cader, M., Matthews, P., *et al.*, 2006. Tract-based spatial statistics: voxelwise analysis of multi-subject diffusion data. *Neuroimage* 31 (4), 1487–1505.

Smith, S., Jenkinson, M., Woolrich, M., Beckmann, C., Behrens, T., Johansen-Berg, H., Bannister, P., De Luca, M., Drobnjak, I., Flitney, D., *et al.*, 2005. Advances in Functional and Structural MR Image Analysis and Implementation. *FMRIB technical report TR04SS2* .

URL `www.fmrib.ox.ac.uk/analysis/techrep`

Smits, M., Vernooij, M. W., Wielopolski, P. A., Vincent, A. J., Houston, G. C., van der Lugt, A., 2007. Incorporating functional mr imaging into diffusion tensor tractography in the preoperative assessment of the corticospinal tract in patients with brain tumors. *American Journal of Neuroradiology* 28 (7), 1354–1361.

Teipel, S., Bokde, A., Meindl, T., Amaro Jr, E., Soldner, J., Reiser, M., Herpertz, S., Möller, H., Hampel, H., 2010. White matter microstructure underlying default mode network connectivity in the human brain. *Neuroimage* 49 (3), 2021–2032.

Terburg, D., Morgan, B., Montoya, E., Hooge, I., Thornton, H., Hariri, A., Panksepp, J., Stein, D., van Honk, J., 2011. Hyper-Vigilance for Fearful Eyes and Improved Recognition of Dynamic Fearful Faces after Basolateral Amygdala Damage. *In review* .

Todd, R., Anderson, A., 2009. Six degrees of separation: the amygdala regulates social behavior and perception. *Nature Neuroscience* 12 (10), 1217–1218.

University of Cape Town

Tuch, D., Reese, T., Wiegell, M., Van J, W., 2003a. Diffusion MRI of complex neural architecture. *Neuron* 40 (5), 885–895.

Tuch, D. S., Reese, T. G., Wiegell, M. R., Wedeen, V. J., 2003b. Diffusion MRI of Complex Neural Architecture. *Neuron* 40 (5), 885–895.

Uddin, L., Supekar, K., Amin, H., Rykhlevskaia, E., Nguyen, D., Greicius, M., Menon, V., 2010. Dissociable connectivity within human angular gyrus and intraparietal sulcus: evidence from functional and structural connectivity. *Cerebral Cortex* 20, 2636–2646.

van den Heuvel, M., Mandl, R., Kahn, R., Hulshoff Pol, H., 2009. Functionally linked resting-state networks reflect the underlying structural connectivity architecture of the human brain. *Human Brain Mapping* 30 (10), 3127–3141.

van den Heuvel, M., Mandl, R., Luigjes, J., Hulshoff Pol, H., 2008a. Microstructural organization of the cingulum tract and the level of default mode functional connectivity. *Journal of Neuroscience* 28 (43), 10844–10851.

van den Heuvel, M., Mandl, R., Pol, H., 2008b. Normalized cut group clustering of resting-state fMRI data. *PLoS One* 3 (4), e2001.

Voineskos, A., O'Donnell, L., Lobaugh, N., Markant, D., Ameis, S., Niethammer, M., Mulsant, B., Pollock, B., Kennedy, J., Westin, C., *et al.*, 2009. Quantitative examination of a novel clustering method using magnetic resonance diffusion tensor tractography. *Neuroimage* 45 (2), 370–376.

Wakana, S., Caprihan, A., Panzenboeck, M. M., Fallon, J. H., Perry, M., Gollub, R. L., Hua, K., Zhang, J., Jiang, H., Dubey, P., Blitz, A., Zijl, P. V., Mori, S., 2007. Reproducibility of quantitative tractography methods applied to cerebral white matter. *NeuroImage* 36 (3), 630 – 644.

Werring, D., Clark, C., Parker, G., Miller, D., Thompson, A., Barker, G., 1999. A direct demonstration of both structure and function in the visual system: Combining diffusion tensor imaging with functional magnetic resonance imaging. *Neuroimage* 9 (3), 352–361.

Woolrich, M., Behrens, T., Beckmann, C., Smith, S., 2004. Mixture models with adaptive spatial regularization for segmentation with an application to fMRI data. *IEEE Transactions on Medical Imaging* 24 (1), 1–11.

University of Cape Town

Yassa, M. A., Muftuler, L. T., Stark, C. E. L., 2010. Ultrahigh-resolution microstructural diffusion tensor imaging reveals perforant path degradation in aged humans in vivo. *Proceedings of the National Academy of Sciences* 107 (28), 12687–12691.

Yu, C., Li, J., Liu, Y., Qin, W., Li, Y., Shu, N., Jiang, T., Li, K., 2008. White matter tract integrity and intelligence in patients with mental retardation and healthy adults. *Neuroimage* 40 (4), 1533–1541.

Zhang, W., Olivi, A., Hertig, S., van Zijl, P., Mori, S., 2008. Automated fiber tracking of human brain white matter using diffusion tensor imaging. *NeuroImage* 42 (2), 771–777.

Zhou, Y., Shu, N., Liu, Y., Song, M., Hao, Y., Liu, H., Yu, C., Liu, Z., Jiang, T., 2008. Altered resting-state functional connectivity and anatomical connectivity of hippocampus in schizophrenia. *Schizophrenia Research* 100 (1-3), 120–132.

University of Cape Town

Appendix A

Default Mode Group fMRI Analysis

Results are presented here for a comparison of patients with UWD with healthy controls during a resting state task. The data were acquired in the same as way as for individual DMN extraction. ICA analyses were conducted on the two groups of subjects using GIFT (Calhoun *et al.*, 2001). Only five of the control subjects were used in order to have matched groups. Data were normalised using intensity normalisation and no scaling was employed. This preserves the relative scaling between subjects facilitating group comparison which was performed as a two-tailed t-test in SPM5. The SPM result for group 1 (Controls) directly compared to group 2 (UWD) is shown in Figure A.1. The results in Table A.1 show a difference with p 0.01 (uncorrected) in the right PCC region, which is a core region of the Default Mode Network.

Figures A.2 - A.5 below show the DMN components for all subjects. The subjects were grouped as follows: subjects 1 - 5: Controls, subjects 6 - 10: UWD). The mean BOLD fMRI time-course is shown in the DMN for each subject.

cluster size	voxel-level p (uncorrected)	coordinates (MNI) mm	Approximate anatomical location
19	0.001	22 -59 22	49% Right PCC cortex (Harvard-Oxford Cortical Structural Atlas)

Table A.1: Summary of significant differences in group analysis of Default Mode Network.

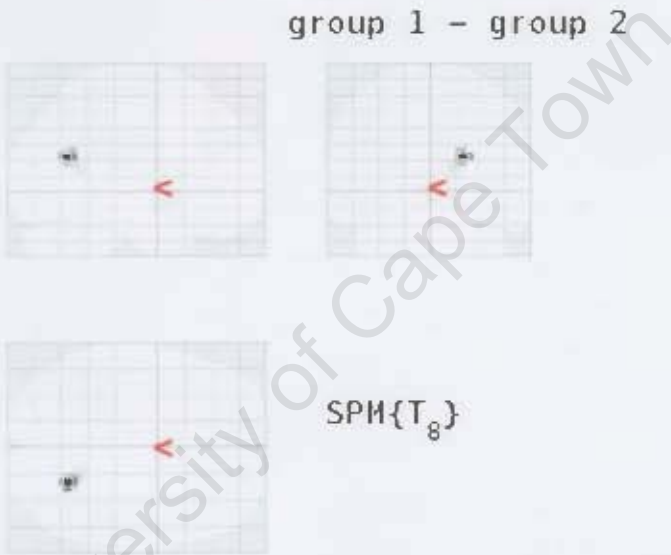

University of Cape Town

Figure A.1: The Default Mode Network group analysis produced significant (uncorrected $p \leq 0.01$) differences for controls versus UWD subjects.

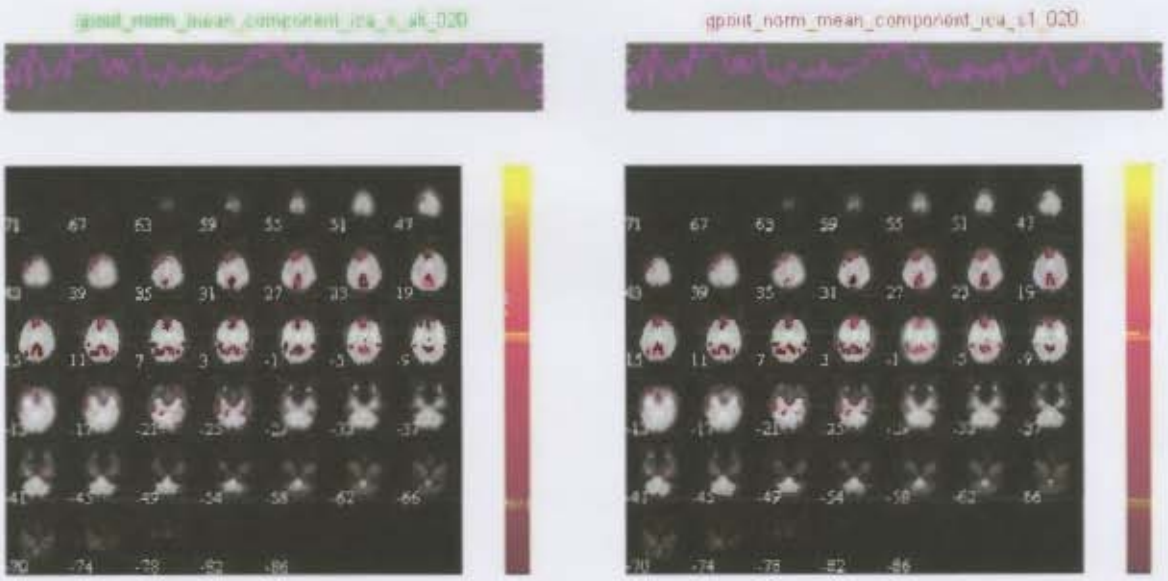

Figure A.2: ICA results - Default Mode Network component for all subjects.

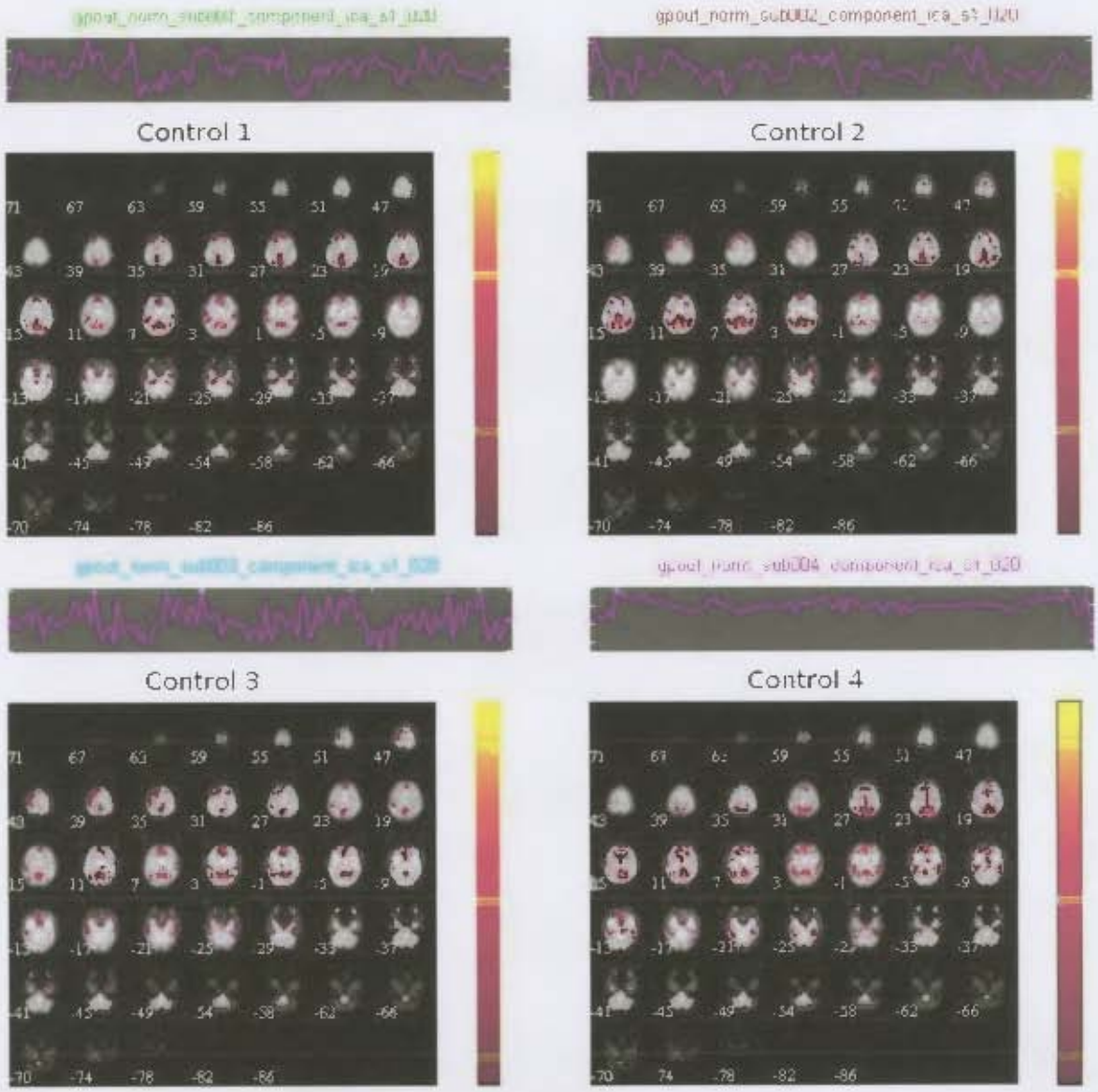

Figure A.3: ICA results - subjects 1- 4.

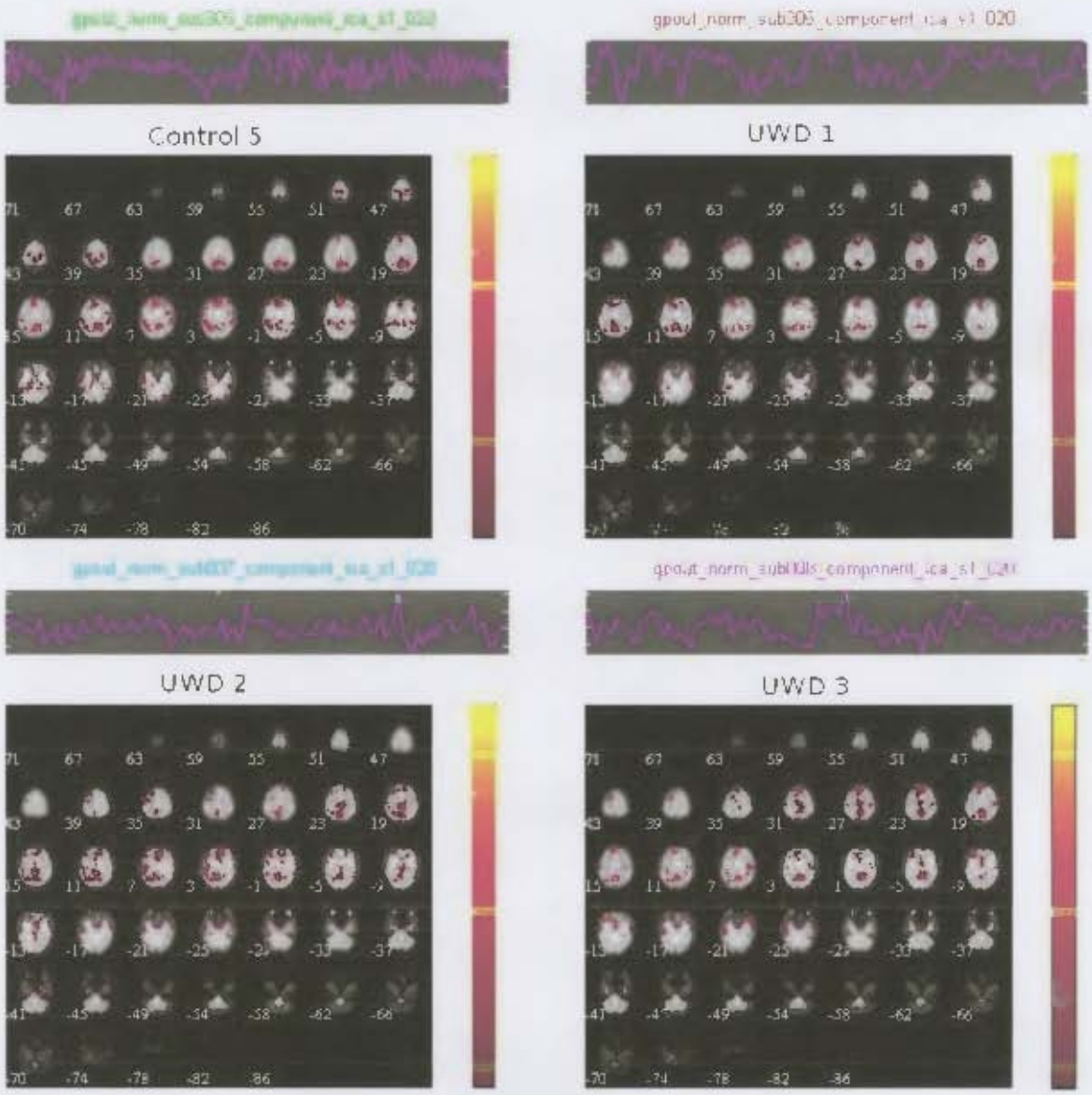

Figure A.4: ICA results - subjects 5 - 6.

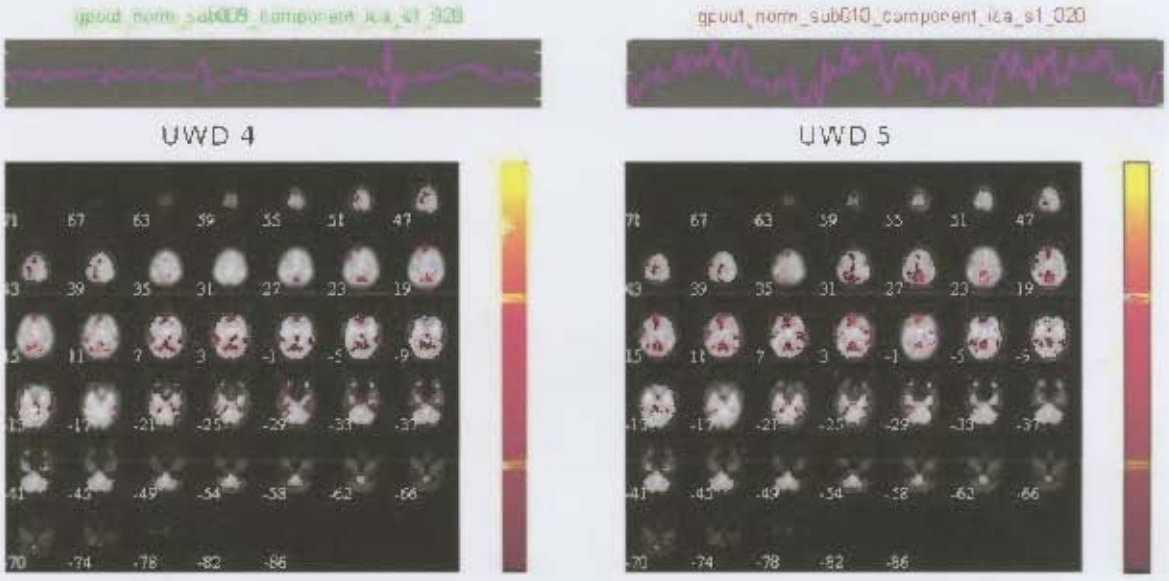

Figure A.5: ICA results - subjects 7 - 10.

Appendix B

Comparing UWD and Control Groups using Tract Based Spatial Statistics (TBSS)

University of Cape Town

Tract-Based Spatial Statistics, or TBSS (Smith *et al.*, 2006), is an automated method which projects individual DTI data onto a common space which allows for statistical testing over the entire brain volume rather than specific tract based methods. It forms part of the FSL toolbox developed by the FMRIB group of Oxford University. FA images are routinely used in voxel-wise statistical analyses to show localised brain changes related to development, degeneration and disease. TBSS is a relatively new technique which has already been applied to a wide range of neurological and psychiatric disorders to assess the micro-structural integrity of white matter. TBSS compliments DTI tractography methods as it offers an alternative data-driven approach to the analysis of DTI data. Only the very centre of the white matter tracts (the skeleton) is considered, thus overcoming the major limitation of standard voxel based statistical analyses, which relates to imperfect coregistration. It can be performed between groups to readily expose white matter differences as measured by differences in FA or other DTI metrics (Arnone *et al.*, 2008).

In order for a statistical model to be compared across different subjects, these images are aligned with one another. The registration algorithms employed create a mapping from the

old voxel positions to new positions in the same coordinate space as a reference image. The target image is manipulated to align with this reference by means of spatial transformations. Aligning FA data from multiple subjects using standard rigid coregistration is not sufficient to align the brains of different subjects, therefore a non-linear registration field is also calculated. This is applied using a b-spline representation of the registration warp field (Rueckert *et al.*, 1999).

First, the "most representative" FA map in the group was found with an exhaustive test to find which image requires the least amount of warping to align all other images to it. This transformation was then combined with the affine transformation required to align the target to standard space.

These tracts were then "skeletonised" by projecting the FA data onto the central portion of the white matter structures, which forms an alignment invariant representation of the tract. This "skeleton" represents the centres of all fibre bundles that are generally common to all of the the subjects. Each subjects' FA data was projected onto the mean FA skeleton in such a way that each skeleton voxel took the FA value from the local centre of the nearest relevant tract. This procedure thus essentially corrects for imperfect alignment. An example FA skeleton is shown in Figure B.1.

After coregistration and skeletonisation, a mean FA image was calculated. A threshold of FA>0.2 eliminated the grey matter and CSF so that the white matter regions were constrained to the regions of the brain that are best aligned. The aligned FA data were then fed into a voxel-wise cross-subject statistical analysis.

TBSS of FA in Urbach-Wiethe Disease

The FA image of each subject was normalised to a $1 \times 1 \times 1$ mm^3 FA template (FMRIB58_FA_1mm) in the Montreal Neurological Institute (MNI) space using the non-linear registration algorithm in FSL (Andersson *et al.*, 2007a,b).

University of Cape Town

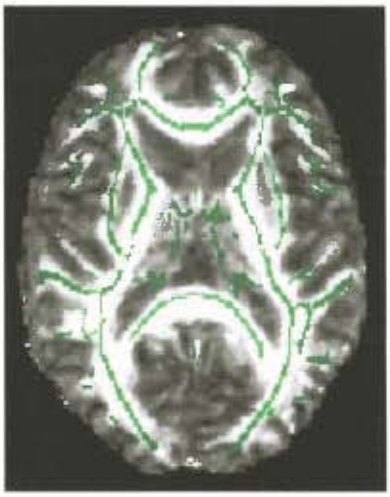

Figure B.1: A mean FA skeleton (green) overlaid on a FA map. In TBSS, the analysis is restricted to the centre of the WM tracts which are "skeletonised" to be represented by a single voxel thick skeleton.

University of Cape Town

The group mean differences were tested using 5000 two-tailed Monte Carlo permutations for the two groups resulting in a voxel-wise p-value image. Significance was considered to be $p \leq 0.05$ Family Wise Error (FWE) corrected. Default Threshold-Free Cluster Enhancement (TFCE) parameters H=2, E=0.5 were used in the analysis.

Results: Urbach-Wiethe Disease Versus Controls

No significant regions were evident when correcting for multiple comparisons with the TFCE algorithm. Using an uncorrected p-value threshold of $p \leq 0.01$, clusters of regions with differing FA are presented in Table B.1. The largest individual clusters are shown in Figures B.2, B.3 and B.4. These results were obtained at $p<0.01$ (uncorrected).

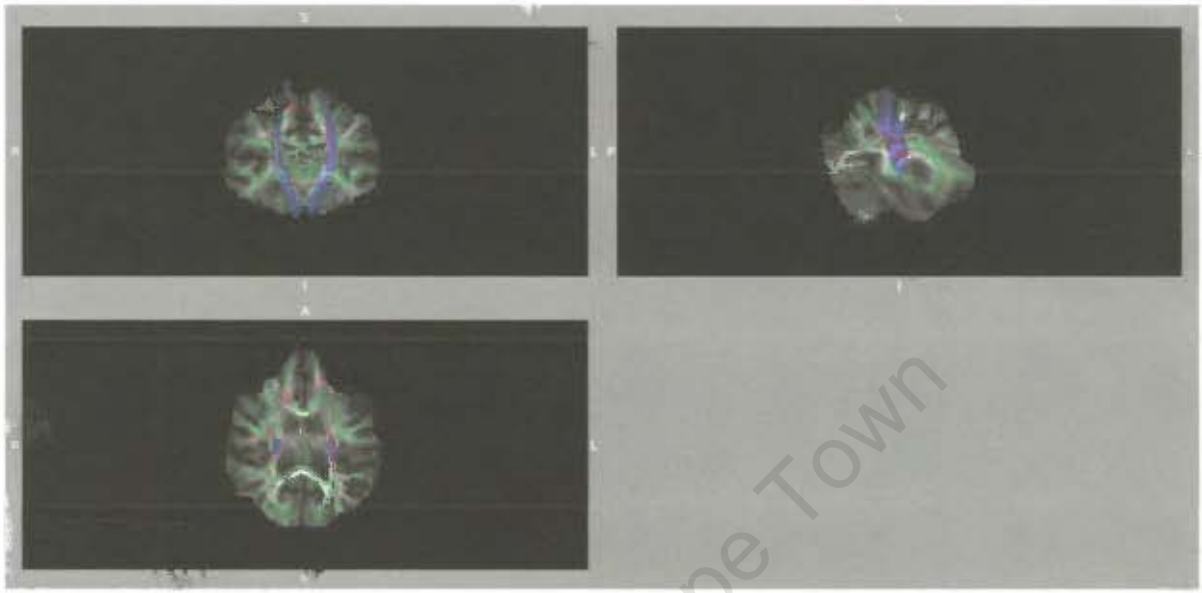

Figure B.2: TBSS DTI results showing FA differences in red at an uncorrected p-value threshold of $p \leq 0.01$. The CST reference from the from the JHU (Johns Hopkins University) white matter atlas is overlaid in blue.

University of Cape Town

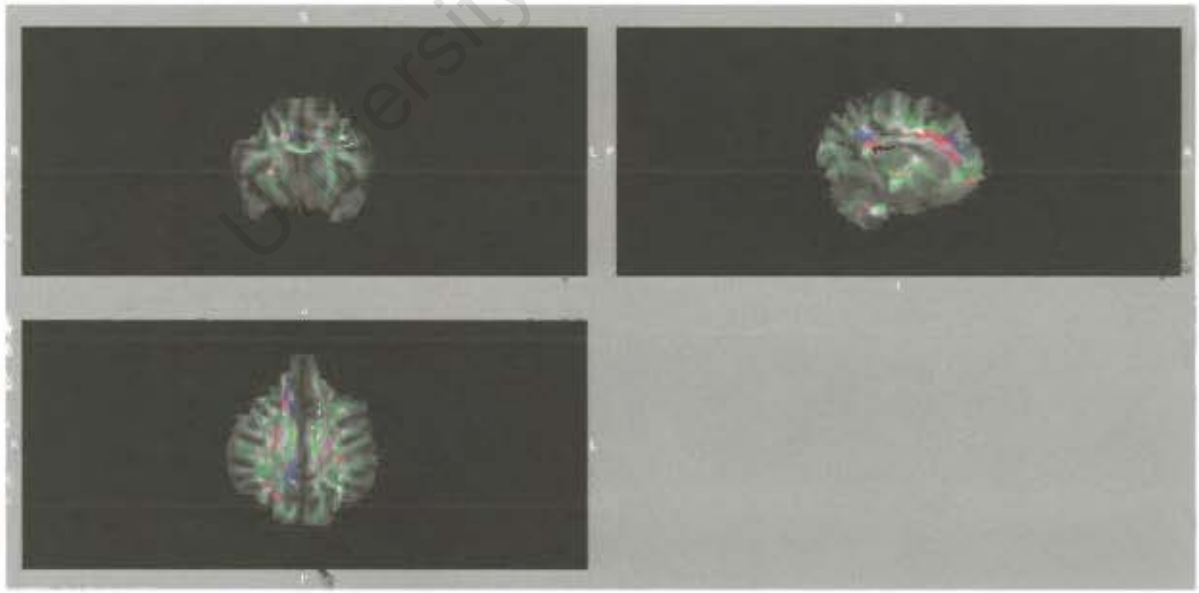

Figure B.3: The right anterior CB shows some FA differences (red), this is shown in relation to the atlas position of the CB in blue. $p<0.01$ (uncorrected).

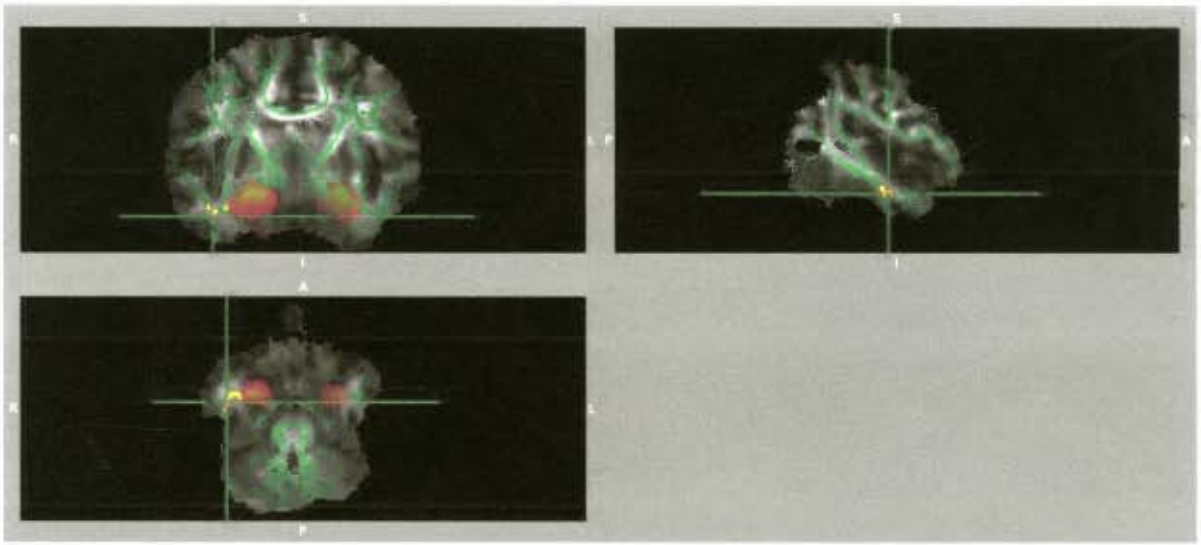

Figure B.4: A cluster of significant TBSS differences was found in the right temporal lobe (shown in yellow). This white matter is part of the uncinate fasciculus. The relation to the atlas location of the amygdala is shown in orange since the uncinate fasciculus connects the amygdala to the PFC. $p<0.01$ (uncorrected).

MNI coords (centroid)			voxels	Z-max	Approximate
x	y	z			Anatomical Location
-22.2	-17.9	24	1235	5.21	Corticospinal tract L
24.7	-13.2	14.2	884	4.46	Corticospinal tract R
16.4	20.6	23.7	767	3.71	Cingulum bundle R
1.45	-24.2	-7.83	275	4.38	Anterior thalamic radiation R
38.5	-5.4	-24.7	243	4.52	Right temporal lobe - uncinate fasciculus

Table B.1: Largest white matter differences from TBSS analysis.